NASA TM-88216

NASA Technical Memorandum 88216

Improved Skin Friction Interferometer

R.V. Westphal, W.D. Bachalo, and M.H. Houser

March 1986

National Aeronautics and
Space Administration

NASA Technical Memorandum 88216

Improved Skin Friction Interferometer

R. V. Westphal, Ames Research Center, Moffett Field, California
W. D. Bachalo,
M. H. Houser, Aerometrics, Inc., Mountain View, California

March 1986

National Aeronautics and
Space Administration

Ames Research Center
Moffett Field, California 94035

This Page Intentionally Left Blank

SYMBOLS

a	beam waist diameter (to $1/e^2$)
C	product of fringe number and time, $C = N_{eff}^* t_{eff}$
C_f	skin friction coefficient, $C_f = \tau/q_e$
C_X	spot location parameter, $C_X = X_1/X_2$
d	distance from focal plane to surface
e	error
f	lens focal length
h	oil film thickness
i	beam intensity
n	index of refraction
N	fringe number; number of optical path lengths in the oil film
P	photodiode output, proportional to light intensity
q	dynamic pressure
r	fringe visibility
s	beam separation due to beamsplitting window
t	time
u,v,w	velocity components in Cartesian system
x	distance from beam waist to lens
X,Y,Z	Cartesian coordinates
α	oil-film wedge angle
δ	thickness
Δ	optical path difference due to beamsplitter
λ	wavelength

μ	viscosity
θ	beam incidence angle (measured with respect to normal local surfaces)
ρ	density
τ	skin friction or shear at air-oil interface

Subscripts

A,B,C,D,E	pertains to light paths depicted in figure 1(b)
a	property of the air
e	pertaining to the freestream of the air flow
eff	"effective" value
ℓ	characteristic of the laser light source
in	input beam properties
o	property of the oil
out	output beam properties
w	property of beamsplitter window
ϕ	value at oil-film leading edge or initial value
1	"upstream"-most measurement position
2	"downstream"-most measurement position

IMPROVED SKIN FRICTION INTERFEROMETER

R. V. Westphal, W. D. Bachalo,* and M. H. Houser*

Ames Research Center

SUMMARY

An improved system for measuring aerodynamic skin friction which uses a dual-laser-beam oil-film interferometer has been developed. Improvements in the optical hardware provided equal signal characteristics for each beam and reduced the cost and complexity of the system by replacing polarization rotation by a mirrored prism for separation of the two signals. An automated, objective, data-reduction procedure was implemented to eliminate tedious manual manipulation of the interferometry data records. The present system was intended for use in two-dimensional, incompressible flows over a smooth, level surface without pressure gradient, but the improvements discussed are not limited to this application.

INTRODUCTION

A thin film of oil on a smooth surface will flow under the action of the aerodynamic shear stress created by the flow of air over the surface. The equations governing the behavior of an oil film in laminar flow are well known (refs. 1-3); figure 1(a) depicts a thin, two-dimensional oil film flowing under the action of aerodynamic skin friction. The skin friction is assumed to be steady in time and constant in the stream and span directions. Skin friction gradients and pressure gradients (including gravity) as well as surface curvature effects are not included; these effects can be included if they are present (refs. 1 and 2). A simple relation then exists between the time-dependent oil film thickness h at a location X and the skin friction:

$$\tau = [(X - X_{\phi})\mu_o]/[h(t,X)t_{eff}] \qquad (1)$$

As this equation gives the time-dependent variation of oil film thickness at a known location and the oil viscosity is known, the skin friction may be calculated from equation (1).

A number of questions remained from previous investigations regarding the response of a flowing oil film to skin friction produced by a turbulent boundary layer. (1) How do the fluctuations in skin friction which are encountered in real

*Aerometrics, Inc., Mountain View, CA.

turbulent flows influence the oil film? (2) Why are "waves" observed in oil films? Both of these basic questions were examined in detail in a companion numerical study (ref. 3) in which it was concluded that the oil film will produce a correct measurement of average skin friction if the average rate of thinning is measured, and that the "waves" are formed from the interaction of the oil film with the turbulent boundary layer. The study also showed that near the oil-film leading edge, there must always be a wave-free region where no interaction takes place and the linear lubrication theory (eq. (1)) is valid. This has also been observed experimentally, although in supersonic flows Monson has found that this region becomes vanishingly small.

To put the method into use for quantitative measurement of skin friction, a technique for accurate film-thickness measurement is required. Wave-free flow at very low Reynolds numbers and the need to confine the film to an area of a few centimeters require oil-film thicknesses of less than 50 μm. Under these conditions, optical measurement using the principle of interferometry is the method of choice.

Although the principle of interferometric film thickness measurement has been known for some time, e.g., Jenkins and White's text (ref. 4), Tanner and Blows (ref. 2) at Brighton Polytechnic were apparently the first to examine quantitative interferometric measurement of oil film thickness as a means for direct determination of skin friction. Murphy and Smith (ref. 5) attempted to apply interferometric film-thickness measurements to obtain evaporation rate data which were to be related to skin friction through a simple mass-transfer analogy. Later, Wazzan et al. (ref. 6) attempted to apply the same technique to a supersonic flow. They actually worked out the relationships of lubrication theory needed to relate the rate of thinning of a liquid film to skin friction, but appear to have overlooked the usefulness of the idea.

The principle of interferometry with a laser beam can be used to measure the time-dependent oil film thickness as shown in figure 1(b). Some of the incident beam is specularly reflected at the air-oil interface (ray A); the remainder passes through the oil film and is either transmitted through (ray B) or is reflected by the solid surface (ray C). The reflected light (ray C) passes through the oil and is partially reflected again at the oil-air interface (ray D--an internal reflection). Multiple internal reflections can be ignored for small reflectance (ref. 4). The transmitted portion of the primary beam (ray E) will interfere with the first (specular) reflection from the air-oil interface, thereby providing a light signal. As the phase relation between A and E changes, the intensity of the signal will vary approximately sinusoidally because of a variation in the optical path length. This variation is caused by a thinning of the oil film. One wavelength in the oil is λ_o (one "fringe"), corresponding to a thickness variation given by references 2 and 4.

$$\lambda_o = \lambda_\ell / [2n_o \cos \theta_o] \qquad (2)$$

where

$$\theta_o = \sin^{-1}[(\sin \theta_\ell)/n_o] \tag{3}$$

Let N denote the film thickness in number of optical fringes, then $\lambda_o N(t,X)$ is equal to the oil film thickness $h(t,X)$. Equations (1), (2), and (3) give the basic equations needed to determine skin friction once the time-dependent fringe history (thickness) of an oil film has been measured at a particular location X. Note that two measurements a known distance apart will be required if the precise location of the oil-film leading edge is not known.

The signal-to-noise ratio is strongly influenced by fringe visibility r, defined as the ratio of the intensities of the two interfering beams

$$r = \min \left(\frac{i_E}{i_A}, \frac{i_A}{i_E} \right) \tag{4}$$

Obviously, maximum visibility is obtained for equal intensity of the interfering beams. The fringe visibility is influenced by the optical properties of both the oil and the surface, as is further discussed later.

Tanner's instrument (refs. 2,7-12) consisted of a fairly small (less than 50 mW) He-Ne laser, beam steering and focusing optics, and receiving optics (fig. 2). A beamsplitter was used to give a second "reference" spot for locating the measuring spot with respect to the oil leading edge. Photodetector output was monitored on a strip-chart recorder and later timed using an analog fringe-detection circuit and a computer (ref. 13). Very long runs were taken so as to thin the oil to less than one fringe. Then, the time at which $N = 1$ occurred could be determined, and a reference fringe number was obtained to allow accurate fringe numbering. Alternatively, the origin for time was taken as the start of the run and the reference fringe number was chosen to give a nearly constant fringe-time product. Measurements were made on coated and uncoated glass as well as on polished metal surfaces. Tanner (ref. 13) also evaluated techniques for viscosity measurement which can be used when oil viscosity is not accurately known. Tanner and his co-workers have done extensive comparisons of the oil-film interferometer technique with the classic Preston tube (refs. 9 and 10), and have also used oil film interferometry for visualization of surface flow patterns (e.g., Tanner, ref. 12).

A "surface phenomenon" was investigated by Tanner (ref. 13). The results indicated that extremely thin films of silicone oil may not accurately follow lubrication theory. These results imply (1) that small-surface roughness (0.2 μm or less) can give rise to an apparent "stagnant" region near the surface and (2) that the oil-film leading edge position is best represented by an "effective" value--probably the result of surface tension. Potential difficulties stemming from (1) are circumvented by the use of very smooth polished surfaces, and by terminating the measurements with a film thickness of approximately 1 μm or so. For the dual-beam system, (2) is automatically satisfied.

Monson and others at NASA Ames Research Center (refs. 14-17) later extended the method by introducing a second data beam, which eliminated the need to locate the leading edge of the oil film. The two data beams were perpendicularly polarized and were separated using polarizing filters. Otherwise, the optical system that was used (fig. 3(a)) was similar to Tanner's. Monson's data-acquisition procedure was to record the output of each photodetector on separate channels of a strip-chart recorder for a period of time sufficient to produce about 20 "good" fringes from the downstream photodetector. The times elapsed for 10 and 20 fringes on the downstream signal were used to calculate the effective time and fringe numbers, thus removing the requirement of using lengthy data records to provide a reference fringe number or of measuring or estimating the time origin. The time elapsed for 10 fringes at the upstream location gave the fringe reference for the upstream beam. The results for the two beams were then combined to give the skin friction. The measurements were made on polished metal test surfaces (aluminum and stainless steel). "Bad" records, defined as those which contained uneven visibility or obvious noisiness, were identified qualitatively by direct inspection of the strip-chart recordings. Figure 3(b) shows a typical signal from Monson's instrument along with the data-reduction equations that were employed for two-dimensional flows with no pressure or shear gradients. They have also used the instrument in a wise variety of flow conditions such as three-dimensional boundary layers, separated flows, and complex supersonic flows.

The present application to skin friction measurements in low-speed, two-dimensional turbulent boundary layers with zero pressure gradient required a measurement uncertainty of ±5%. Discussions with Monson (private communication) and the authors' initial tests of a prototype single-beam system revealed a number of problems with the existing instrument. Usual data-reduction procedures called for tedious and somewhat subjective manual manipulation of fringe records. "Bad" runs were often obtained and later discarded, and the fringe visibility index was quite low ($r < 0.2$) because metal test surfaces were used. Monson's system gave a different signal quality for each beam (fig. 3(a)), which tended to complicate processing of the fringe records. Monson also indicated that oil heating could be produced by the use of highly focused beams if too much laser power was employed.

Two major objectives evolved for the current work. The first was to design and build a new two-beam interferometer that would give matched signal quality on both beams. Maximum fringe visibility was sought to give the best signal-to-noise ratio and to allow the use of the least amount of laser power (thereby minimizing oil heating). The second objective was to automate the fringe processing procedure to remove any subjectivity in the identification of bad records and to speed the data processing so that skin friction could be measured on-line during an experiment. Initially, an uncertainty analysis was carried out to establish requirements for tolerances and design parameters. This analysis is described in the next section, followed by sections which outline the optical hardware and data-reduction procedures. Problems encountered with the system, as well as sample results, are given in the Discussion section. The Concluding Remarks include the authors' plans to implement further refinements to the interferometer.

The authors are grateful to Mr. D. J. Monson of NASA Ames Research Center for helpful discussions on many aspects of interferometric skin-friction measurement. The work of Mr. T. M. Lichtenstein and Mr. C. Hooper on the data-acquisition software system, and the efforts of Mr. Rich Piquette on coating the glass inserts, are also acknowledged.

UNCERTAINTY ANALYSIS

An uncertainty analysis was undertaken to aid in the design and to point out critical measurands. Combining (1) and (2) and then introducing the (constant) product of fringe number and time C gives

$$\tau = \mu_o(X - X_\phi)/[\lambda_o C(X)] \tag{5}$$

Applying (5) for each beam to eliminate X_ϕ gives the dual-beam data reduction equation

$$\tau = \mu_o(X_2 - X_1)/\{\lambda_o[C(X_2) - C(X_1)]\} \tag{6}$$

The uncertainty in τ can be evaluated by a simple root-sum-square combination of the uncertainties from the individual terms under the assumption that these terms are mutually independent (ref. 18). For the present application, the uncertainty is expressed as a percent of the indicated value and all values are estimated at 20:1 odds. The analysis is summarized in table 1, in which the partial derivatives and uncertainties in each term are individually evaluated. Four separate terms are identified and discussed below.

Oil viscosity appears as a linear term in equation (6) and therefore contributes strongly to the uncertainty. Tanner (ref. 13) and Monson (ref. 14) both directly measured the viscosity of the oils they used; Monson's measurements were used in this analysis. Fifty-centistoke (cs) (nominal) oil such as Monson used (ref. 14) was obtained, the viscosity of which was found to conform to within 2% of the manufacturer's quoted values (see fig. 4 of ref. 14). The manufacturer's relation for viscosity was adopted

$$\mu_o = \mu_{nom} \exp(-0.0146(T_o - T_{nom})) \tag{7}$$

Oil temperature was assumed to be equal to the flow temperature, which was continuously monitored during each experiment. When the temperature drifts or the flow is not isothermal, special treatment is required as the oil viscosity changes rapidly with temperature. Generally it is necessary to measure the oil temperature more directly (e.g., with a temperature probe embedded in the surface below the oil).

Beam spacing $(X_2 - X_1)$ also appears as a linear term in equation (6), and was measured directly to an estimated uncertainty of 0.05 mm, or about 2% for the smallest spacing used (2.77 mm). The measurement was made using a diffuse surface placed

at the spot focal plane. Repeated trials were averaged to yield the quoted uncertainty.

Alternatively, if oil viscosity was measured directly by one of the techniques employed by Tanner (ref. 13), the instrument could simply be calibrated in terms of the product of beam spacing and viscosity. This procedure may somewhat reduce the net uncertainty.

The uncertainty in the optical path length in the oil depends primarily upon accurate knowledge of the oil index of refraction, because the laser wavelength is known precisely and the incidence-angle term $\cos \theta_o$ is very nearly unity for near-normal incidence. The oil index of refraction, which was nominally 1.4, was measured as 1.405 using an Abbe refractometer. The uncertainty in this measurement is estimated to be less than 0.5%--leading to an uncertainty in λ_o that is negligible compared to the other terms.

The fringe-time products $C(X_1)$ and $C(X_2)$ are the primary measurands of the system. The difference of these two quantities has been considered a single term for convenience. It is apparent from table 1 that the net-uncertainty contribution from this term depends upon the selection of measurement location if the uncertainty in the determination of C is taken as a fixed percentage of the value. The results showed that as long as more than 20 fringes were used, the value of C could be determined with an estimated uncertainty of about 0.5%. This estimate was obtained from experiments with two-dimensional flat-plate boundary layers with minimal gradients of pressure and skin friction at shear levels of 0.5 to 2 N/m^2. For a 3% to 4% uncertainty contribution from this term, this estimate implies that the value of $(X_1 - X_\phi)$ should be less than about four times the beam spacing.

The minimum value of $(X_1 - X_\phi)$ was determined by the requirement that more than 20 fringes be identified. The limited spatial resolution caused by the finite spot size of the beams caused reduced fringe visibility if the oil-film wedge angle was greater than approximately 0.1°. Twenty fringes correspond to a thickness of approximately 5 μm. This thickness implies that the minimum distance to the leading edge should be approximately 3 mm, which was approximately equal to the smallest beam spacing that was used.

These uncertainties indicate that the minimum uncertainty likely to be attained with the oil-film-interferometry technique is about 3%, which is primarily caused by the uncertainty in the determination of the oil viscosity. The analysis shows that the main contribution to the uncertainty for the current instrument is the uncertainty in the determination of the difference in the finge-time product at the two measurement locations. This uncertainty may be limited to 3% to 4% if $(X_2 - X_1) < (X_1 - X_\phi) < 4(X_2 - X_1)$ is maintained. The overall uncertainty in measurement of skin friction, subject to the assumptions outlined above and valid for the system described below, is estimated at approximately 5%.

OPTICAL HARDWARE

A photograph and schematic of the optical system are shown in figure 4. As in previous configurations, the current system transmits two beams focused onto the test surface and uses PiN photodiodes as the detectors. Both transmitter and receiver components share a common optical-rail assembly. The test beams pass through a slot in the rail with the test surface located below the optical assembly. Light scattered from the surface is collected through the same slot so that the test beam incidence must be near-normal to the surface (actual incidence angles were about 3°). The key optical-design change from previous work is the physical separation of light that is reflected from the two surface spots through the use of imaging lenses and a reflective edge. This change allowed for simplification of the optical system and maintained good separation (minimal crosstalk) between the two channels.

A low-power (0.8 mW), polarized, helium-neon laser provided the coherent light source. The beam is directed by mirrors through a beam-expanding and -focusing telescope, composed of a 20-power microscope objective and a 150-mm-output lens. By adjusting the separation between the objective and output lenses, a focused spot was produced on the test surface at a considerable distance from the output lens. The equations which describe the transformation of the (approximately) Gaussian laser beam are

$$a_{out} = \frac{f a_{in}}{\left[(x_{in} - f)^2 + \left(\frac{\pi a_{in}^2}{\lambda_\ell}\right)^2\right]^{1/2}} \tag{8}$$

$$x_{out} = f + \frac{(x_{in} - f) f^2}{(x_{in} - f)^2 + \left(\frac{\pi a_{in}^2}{\lambda_\ell}\right)^2} \tag{9}$$

Applications of these equations with values for the actual optical configuration yielded a focused beam diameter of approximately 42 μm.

After leaving the beam expander, the beam is directed onto a plane-parallel to 10 arc-sec) window of known thickness. At an incidence angle of 45°, both the front and back surfaces of the window reflect about 4% of the incident beam. This arrangement splits the expanded beam into two test beams of nearly identical intensity, with a separation given by the following equation:

$$s = \frac{2\delta_w \sin \theta_\ell}{\tan \cos^{-1} \frac{\cos \theta_\ell}{n_w}} \tag{10}$$

A fixture was fabricated that allowed windows of different thicknesses to be interchanged, which produced spot separations in the range of 2 to 10 mm.

The beamsplitting method just described introduced a difference in optical path length between the two test beams. This difference, which changes with the window thickness, is given by

$$\Delta = \frac{2n_w \delta_w}{\sin \cos^{-1} \frac{\cos \theta_\ell}{n_w}} - \frac{s}{\tan \theta_\ell} \tag{11}$$

The consequence of the path difference is a change in focus location, which prevents focusing both beams simultaneously on the test surface. It is not critical that focus occurs at the test surface, but it was considered desirable to produce two spots of equal size. In practice, the beam expander was adjusted to equalize the resulting spot sizes at the test surface. This "out-of-focus" condition produced one beam focused above the test surface and the other beam focused below the test surface. The change in beam diameter with distance from the focal plane is given by

$$a(d) = a_{in} \left[1 + \frac{\lambda d}{\pi a_{in}^2}\right]^{2\ 1/2} \tag{12}$$

Most of the testing was done with a BK-7 window of a nominal thickness of 3.2 mm, which introduced a path difference of about 8.5 mm. Proper adjustment of the beam expander would therefore produce two spots on the surface, each located 4.25 mm from the focal plane. The results of the application of equation (12) indicate that this condition will produce surface spot sizes of 92 μm--about double the focused spot size.

After the beamsplitting was performed and the component losses were taken into account, each of the two test beams contained less than 3% of the original laser power--24 μW per beam for the present system. This resulted in a surface-power density of less than 0.004 W/mm^2 per spot, which minimized oil-film heating but still provided sufficient signal amplitude for the detectors.

The receiving system consisted of a 450-mm focal length lens which collimated both specular and diffuse reflected light. A second lens (f = 250 mm) focused the light from the two spots onto opposite sides of the edge of a reflective-coated, right-angle prism. Sufficient image separation and spot focus allowed redirection

of the light from the two surface spots to individual detectors. An adjustable iris and laser line filter preceded each detector to minimize background light detection. The photodetectors were identical photodiodes of the PiN type with active areas of 1 cm^2 and sensitivity of 0.4 μA/μW. The photodiodes were operated in the photovoltaic mode by identical, battery-powered amplifiers and had a saturation level of 50 mW/cm^2. An amplifier gain of 10 V/μA was used, which yielded signal levels of a few volts that were convenient for direct input to the computer analog-to-digital (A/D) converter.

SIGNAL PROCESSING AND DATA REDUCTION

The computerized data-acquisition system (shown schematically in fig. 5) consisted of a PDP 11/44 minicomputer with 20 Mbytes of hard disk storage and a clock-driven, fully differential eight-channel A/D converter. The analog outputs from each photodiode amplifier were simultaneously read directly by the A/D converter for a period sufficient to record 4000 samples per channel. The sample rate was selected (through variation of the clock frequency) to record a sufficiently long fringe record so that a thinning of the oil to about 1 μm could be achieved at the measurement location farthest downstream. These data were written directly to hard disk, then processed on-line with a separate data-reduction program that included graphics capability.

Figure 6(a) shows a typical raw digitized data record from the two photodetectors. The data-reduction procedure described in this section details the method used to process such records to obtain the value of C (the constant product of fringe number and time discussed in the section on uncertainty analysis). Note particularly that each channel is treated independently, i.e., the product of the fringe number and the flowing time for the upstream and downstream channels are computed independently by using the same reduction parameters. An unexpected side benefit of this fitting procedure is that the fitting parameters give an objective measure of the data quality and therefore a criterion for the rejection of bad records, as explained further in the next section. Then the results from the two beams are combined, along with the optical system parameters, oil properties, and tunnel conditions to compute the skin friction. The Appendix contains listings of the computer routines (referenced in this section) which were used to perform the data reduction. Other aspects of the data acquisition, graphics, and database management software used with our particular hardware are described in a separate report (ref. 19).

In the data-reduction procedure, the fringe locations are identified and then the locations (in time) of successive fringes are fitted to the lubrication theory with a best-fit criterion. First, the digitized photodetector output is smoothed using either an exponential or multipoint smoothing algorithm (both algorithms were included in subroutine SCSM00). It was soon concluded that smoothing was not necessary because the fringe identification algorithm provided some smoothing and

the photodetector output was virtually noise-free. Whenever smoothing was used, exactly the same algorithm and parameters were used for each channel.

A simple fringe-identification algorithm was developed and implemented in subroutine SCZERO. A fringe location is most accurately defined as a location where the signal amplitude equals its mean level (a "zero crossing," rather from a signal peak). This definition is the same as that used by Tanner, but different than that of Monson, who used signal peaks. It was decided to use only positively sloped zero crossings so that successive zero crossings corresponded to reductions in film thickness of precisely one fringe. The zero finder algorithm worked by first determining the mean signal level and standard deviation (fig. 6(b)). Next, regions where the data values fell within a specified fraction of 1 standard deviation (SD) of the mean line were bracketed. Finally, the data in each identified region were fitted to a straight line whose intercept with the mean line was taken as the fringe location. Note that the algorithm does not account for possible drift in the mean line.

A minimum-error fitting procedure was used to select the best value of the fringe-time constant C for each beam (subroutine SCCFIT). Each successive zero crossing corresponds to a reduction in oil-film thickness of one fringe, so the film thickness in fringes at the kth zero crossing is simply

$$N_{eff}(k) = N_{\phi} - k \tag{13}$$

Similarly, the effective time of flowing can be defined as

$$t_{eff}(k) = t_{\phi} + t_k \tag{14}$$

where N_{ϕ} is the reference fringe number and t_{ϕ} is the time constant. The values of N_{ϕ} and t_{ϕ} were chosen to minimize the relative error (e) in the resultant value of $C(X)$, that is, t_{ϕ}, N_{ϕ} so that

$$e = \frac{\overline{C^2} - (\overline{C})^2}{\overline{C}} \tag{15}$$

is minimum, with

$$C_k = N_{eff} \cdot t_{eff}$$

and

$$\overline{C} = \frac{1}{k_{max}} \sum_{k=1}^{k_{max}} C_k$$

$$\overline{C^2} = \frac{1}{k_{max}} \sum_{k=1}^{k_{max}} C_k^2$$

Equation (15), with the minimization constraint, is the fitting equation mentioned below.

Both data channels were analyzed by using equation (15), with the minimization constraint, which gave reference values N_ϕ and t_ϕ for both data beams. This analysis contrasts with Monson's procedure, which computed the effective oil-flow time reference from the downstream beam only, and that of Tanner, who generally used an actual time of flow. The new method gives the effective time from the least-square fit for each channel. The two values of t_ϕ were then compared; substantial differences in these constants are taken to indicate bad data, as explained further in the next section. Figure 6(c) shows the results of fitting the fringe data of figure 6(b) in this manner; it can be seen that $1/N_{eff}$ is precisely a linear function of t_{eff}.

Note that the fringes whose amplitude is less than the specified fraction of an SD that is used to bracket the zero-crossing region cannot be identified. This means that for records which contain highly variable fringe visibility, fringes will be missed. These records were found to yield a poor fit to lubrication theory, i.e., a large value of the error e defined in equation (15). It was found that most records yielded $e < 0.003$, and that $e > 0.004$ signaled that fringes were missed, or that dirt was present on the oil.

This fitting procedure is applicable only to the case of two-dimensional flow with no pressure or skin-friction gradients in the streamwise direction and no body forces (such as grvity). If such effects are present, the fitting equation must be modified to account for them. However, the data-acquisition and fringe-identification procedures just described should still be applicable. A suitable minimum-error fitting criterion is substituted for that defined by equation (15). For example, appropriate equations are given by Tanner (refs. 2 and 7) for several combinations of effects; Monson (ref. 17) has investigated applications to three-dimensional flows in detail.

After $C(X_1)$ and $C(X_2)$ are found through the fitting procedure just described, subroutine SCLOFI is used to implement equation (6) with the additional input values of the free-stream dynamic pressure of the tunnel, the oil temperature, the beam spacing, and the incidence angle. The Dow-Corning viscosity relation (eq. (7)) is implemented in this routine.

DISCUSSION AND SAMPLE RESULTS

As with any measurement procedure, experience in the laboratory with this procedure disclosed several unanticipated characteristics. These are discussed with the goal of anticipating similar problems in future applications of the method. None of these characteristics represented major impediments, but they did affect the procedures and equipment finally settled upon. These problems will first be discussed; example measurements will then be presented.

Method of Oil Application

Oil is first applied to the surface. Then the tunnel is turned on and allowed to achieve the test speed. During this start-up period, the film thickness rapidly attains the linear distribution of lubrication theory. For two-dimensional flow, the initial, streamwise, oil profile was found through direct calculation to have no effect on the results (ref. 3). It has no effect because the linear thickness distribution near the leading edge is very rapidly established and the early-run data (while the film is relatively thick) are not used. The procedure presented in this paper in which the effective oil-flow time and reference fringe number are computed from only a segment of the fringe record further contributes to the insensitivity of the results of the fit to initial conditions at tunnel start-up.

Theoretically, in the absence of gravity and surface tensile forces, the initial spanwise extent and uniformity of the film should also be unimportant. Monson (ref. 16) observes that measurements using drops of oil will suffice for measurements in two-dimensional flows. It was assumed that the presence of both finite surface tension and gravity effects would imply the use of oil films that were at least several times the beam spacing in spanwise extent. Monson (refs. 14-17) used a plastic straight edge which was coated with oil and then pressed onto the test surface; this method was found to be tedious in application. To aid in the application of a uniform, initial oil line, a fixture was used (fig. 7) which consisted of a syringe and a metal wedge with a small slit. Using this fixture, repeatable and uniform oil lines about 4 cm long which contained approximately 0.05 cc of oil could be applied.

Dirt on the Film

The presence of dirt or dust specks on the oil surface is the single most important consideration in the application of the oil film method. Small particles can deflect the laser beam or can cause local distortion of the oil flow and consequent behavior which deviates from lubrication theory. In the experimental design, it is desirable to minimize the occurrence of dirt on the oil film surface and to identify or note the presence of dirt so that contaminated data records can be discarded. Dirt on the film was minimized by using filtered air in the wind tunnel and by carefully cleaning the test surface. Use of the oil applicator described earlier also helped maintain oil purity by preventing any contact of the dust-laden air with the (clean) oil.

Dirt recognition proved to be a more serious problem. Initially, the oil film was inspected visually after each run for specks of dirt. However, about half the runs revealed some amount of dirt, although it often was far from the measurement location. The dirt-contaminated records always displayed erratic fringe patterns. Every attempt to fit these records to lubrication theory resulted in large errors and/or unequal values of the time constant t_ϕ from the two beams. This result led to the adoption of two criteria for the rejection of "dirty" signal records:

1. If $e > 0.004$ for either beam; or

2. If $|t_{\phi,1} - t_{\phi,2}| > 0.02\ t_{eff}@(k = 1)$.

These relations represent a completely objective criterion for rejecting bad data records in a systematic way. Use of the above criteria resulted in a rejection rate of approximately 15% to 20%, which is a significant improvement over the 50% rejection rate obtained from visual inspection of the oil film. If the rejection were based on visual inspection of the fringe records for anomalous behavior, up to twice as many runs would be rejected if one were discriminating in the inspection.

Test Surface Finish

Tanner (ref. 12) has reported that the best fringe visibility occurs if partially reflective, metal-coated glass surfaces are used because the oil-free surface reflects only 4% (approximately) of the incident beam. To achieve maximum visibility ($r = 1$), the reflectance at the oil-wall interface should also be about 4%. The reflection from a polished metal surface is composed of specular and diffuse components. Surfaces that are highly polished will reflect specularly a higher proportion of the incident beam. Tanner (ref. 12) reports that excessively polished surfaces will give too much specular reflection, thereby causing multiple internal reflections which degrade signal quality (see also ref. 4). Only the specular reflection from the polished surface will interfere with the (specular) reflection at the air-oil interface. It would therefore seem that the polish need merely be adjusted to give the proper proportion of specular reflection.

Polished aluminum inserts were initially used for the measurement surface beneath the oil film. However, it proved extremely difficult to obtain a consistently uniform finish over the entire surface and to repeat signal quality from day to day. With the fairly short-focal-length optical system and moderately large beam expansion, significant "speckle" was present in the collected light. The speckle pattern, the well-known result of diffuse reflection near the focal plane (ref. 20), would often overwhelm the fringe signal with its intensity.

In view of these difficulties, the metal-coated glass inserts shown in figure 7 were adopted. The test surface was coated with pure chromium by using vapor deposition; a reflectance of 0.2 to 0.4 was achieved, measured with a He-Ne laser beam at normal incidence in air. This gave a fringe visibility in the range $r = 0.5 - 0.7$. Chromium, which has also been used by Tanner (ref. 12), was selected because of its excellent abrasion resistance--one coated insert has been cleaned over 200 times with no detectable degradation in surface reflectance. The back surface was treated with an antireflective coating of $MgFl_2$, which was cured at an elevated temperature. Figure 8 contrasts the best signals that were obtained from the polished aluminum inserts to those that have typically been obtained with the metal-coated glass inserts.

Pure sapphire would also be expected to give reasonably good fringe visibility because of its high refractive index. Also, several commercial optical-coating

shops offer highly abrasion-resistant dielectric coatings which can be tailored to give the correct reflectance in oil, although the cost of this alternative is about five times that of chromium coating. For large surfaces, vapor-deposition is not practical because of the limited size of the coating apparatus. However, it may be possible to use a polymer film if its surface is treated appropriately. Uncoated optical glasses generally have refractive indices very near those of silicone oils (silicone oils have 1.4), so fringe visibility on these surfaces is quite low. If polished metal surfaces must be used, collection of the diffuse reflection must be minimized, e.g., by the use of a small collection aperture with less beam expansion and a longer focal length. Even with these precautions, erratic fringe visibility and subsequent higher data-rejection rates must be anticipated when metal test surfaces are employed.

Vibration of the Instrument and Test Surface

The interferometer system is not inherently sensitive to relative vibration between the instrument and the test surface, because such vibrations do not disturb the relative phase of the two interfering waveforms. However, two important cases in which vibration was important were noticed--one related to the use of detector apertures and the other to cases with substantial diffuse reflection.

Detector apertures were used to effectively reduce the spot size, thus giving improved spatial resolution. This feature proved especially helpful for cases in which the oil film wedge angle exceeded approximately 0.05°. This optical configuration is mildly sensitive to vibration because of the relative motion of the expanded spot on the detector aperture, which creates a change in the total light intensity that is incident on the photodiode. The instrument was clamped securely to the tunnel support rails, which alleviated the problem.

Whenever significant amounts of diffuse reflection were present in the collected light and the sending optics focused the incident beam on the surface, the interferometer was extremely sensitive to the small vibration caused by the tunnel motor. This effect was traced to the speckle pattern created by diffuse reflection from the metal surface, which changes radically with the distance from the focal plane to the surface plane. In fact, the interferometer essentially behaves as a vibration measurement apparatus (ref. 20) under these conditions. As explained above, this situation arises when metal test surfaces are used and is accentuated by short, highly expanded, focused optical systems. All measures to alleviate the problem--longer focal lengths, unfocusing, and smaller beam expansion--resulted in a sacrifice of spatial resolution. The use of the coated glass inserts avoided the problem of speckle noise.

Laser Output Intensity Drift

Most He-Ne laser manufacturers specify that the total laser-beam-output power, after a short warmup period, will remain constant to within ±5%. Tests of three

different manufacturers' units of the 1-mW range verified the accuracy of the specification. However, the time period of the output power variation proved to be in the range 20 to 200 sec, which was comparable to typical periods between fringes in our experiments. Thus, it was not feasible to remove the small mean drift via bandpass filtering. Implementation of a method of tracking the mean signal level by finding the local maximum and minimum levels proved cumbersome to implement. Instead, the "scatter" (estimated at about 5%) which this problem introduced into the results was figured in by taking several measurements (about five) at each measurement point and averaging the results. This procedure had the effect of reducing the uncertainty in the determination of the term $[C(X_2 - C(X_1)]$ from about 5% to about 2% to 3% so that the overall uncertainty in the measurements was still estimated to be about 5%.

Example Results in a Turbulent Boundary Layer

Measurements were made in the Boundary Layer Wind Tunnel operated by the Fluid Dynamics Research Branch at NASA Ames. The test surface in the facility is level to within 0.1° and the static pressure varied less than 0.5% of the free-stream dynamic pressure. The test section is 80 cm wide and 300 cm long, with an adjustable height (20 cm nominal) for pressure-gradient control. The test-wall boundary layer was tripped using a 0.4-mm-diameter wire located 20 cm from the inlet. Optical access for the interferometer was through the transparent Lexan control walls opposite the test surface. After the interferometer was moved to a particular measurement location and securely bolted to the tunnel-support rails, it was carefully focused on the surface and realigned. This procedure typically took about 20 min.

The measurement procedure was as follows: (1) the insert was removed from the tunnel, cleaned with both acetone and lens-cleaning solution, and then wiped and blown clean with canned, dry compressed air. (2) Oil was applied as was described in the Oil Applications section using the special applicator fixture. (3) With the tunnel off, the insert was installed into the test plate and bolted securely into place. The insert was installed flush with the surrounding test plate to within 0.02 mm. (4) The tunnel was turned on and brought to the test condition within about 15 sec. Data acquisition was initiated only after the test condition was established. The set-point free-stream velocity was maintained to 0.25% and the temperature to within 0.2°C over the period of data acquisition.

Data reduction was accomplished using the laboratory computer. First, the digitized photodetector signals were displayed on the graphics terminal, and a contiguous portion of the record was selected where the fringe visibility was nearly constant for both beams. The record selected was generally about 75% to 90% of the entire record acquired. Fringe identification and the fitting of the fringe times to lubrication theory was then accomplished. Plotting of the fitted data was provided to verify that no fringes were missed, although the constraints for equation (15) also identified such records. Records meeting the constraints for equations (15) above were rejected; otherwise, the results $C(X)$ from each beam were combined with the other measured parameters to yield the skin-friction

coefficient. Measurements were repeated five times at each measurement condition and averaged.

Data shown in figure 9 were obtained under the conditions summarized below.

Oil nominal viscosity	50 cs at 25°C
Data record length	400 sec
No. fringes per record	20 to 40
Freestream dynamic pressure	1.8 ± 0.1 in. H_2O
Flow temperature	10° to 20°C
Beam spacing	2.77 mm
Beam position ($X_1 - X_\phi$)	3 to 8 mm
Glass insert reflectance	20% to 40%
Aperture diameter	1.5 mm

For comparison, skin-friction estimates were also obtained by fitting measurements of the boundary-layer mean-velocity profiles to the Law of the Wall-Wake (ref. 21). The results shown in figure 9 indicate agreement between the two techniques to within 5%, which supports the uncertainty estimate given in the section on uncertainty analysis. The time required to obtain these data is comparable (1) because the optical system at each station must be realigned and (2) because five oil-film measurements must be averaged so as to mitigate the effects of laser power drift. However, the laser oil film interferometer is a direct measurement technique--not subject to any assumptions regarding local-profile similarity--and is therefore much more widely applicable than the Law of the Wall-Wake.

CONCLUSIONS

An improved skin-friction laser interferometer system has been designed and tested. Uncertainty estimates have been used in designing the instrument and have been verified. A new fitting procedure developed for data analysis yielded the unexpected benefit of providing an objective, easily implemented method for rejection of "bad" data records thought to be primarily the result of dirt accumulation. The final data-reduction equation used thus far was limited to the single case of constant pressure with two-dimensional flow, without gradients of pressure or skin friction and excluding body forces (e.g., gravity).

Further refinements to the system are being pursued. (1) An automatic oil-application system is being developed which will allow oil to be injected under conditions of flow in the tunnel. (2) A third data beam, with a third photodiode placed behind the beamsplitter, is being added to monitor the laser-output power level. This information will be used to directly measure the mean output level, which should eliminate the need for multiple measurements. (3) Use of a larger beam expander and closer beam spacing are being examined in an effort to improve spatial resolution.

APPENDIX

Four computer routines for processing the digital photodetector signals are included. These are listed below along with the function of each routine.

1. SCSMOO: Digital smoothing of the photodetector output

2. SCZERO: Fringe identification algorithm

3. SCCFIT: Curve fit to lubrication theory

4. SCLOFI: Calculation of skin friction coefficient

```
      SUBROUTINE SCSMOO ( IRAWDT, NRAWMX, FACTOR, MODE )
C
C ACRONYM:  Standard Computations - SMOOth data
C           -        -               ----
C
C PURPOSE:
C       Smooth the data array - value of MODE determines the type
C       of smoothing algorithm employed.
C
C       For 3-pt. smoothing algorithm, MODE determines the no. of
C       times to loop through.
C
C METHOD: self explanatory - see NOTES and code
C
C ARGUMENTS
C    ARG        DIM      TYPE I/O/S DESCRIPTION
C   IRAWDT     NRAWMX     I    I/O  The raw data to be smoothed - the smoothed
C                                    results are written back into the same
C                                    raw data array.
C   NRAWDT       -        I     I   Length of IRAWDT array.
C   FACTOR       -        R     I   Smoothing factor: (for MODE=1)
C                                       1.= Perfectly flat curve
C                                       0.= No smoothing
C                                       Values between 0. and 1. give varying
C                                       degrees of smoothing.
C   MODE         -        I     I   Determines type of smoothing to use :
C                                     0 = single-pole or "causal" exponential
C                                         smoothing with parameter FACTOR.
C                                     1 to 10 = 3-pt. smoothing formula
C
C COMMONS USED: None
C
C FILES USED: None
C
C ERROR HANDLING: None
C
C NOTES:
C (1)   This routine modifies the input (raw) data array.
C (2)   With MODE=0, a fixed time delay is introduced into the data,
C       visisble as a rightward shift of a few sample intervals.
C (3)   For MODE=1 to 10, no phase distortion (time delay) accrues
C       from filtering.
C (4)   Successive applications of the 3-pt. algorithm simply provide
C       higher-order smoothing, i.e., 3-pt. smoothing used twice is
C       precisely 5-pt. smoothing.
C
C LOCAL VARIABLES:
C    VAR        DIM      TYPE DESCRIPTION
C   SMOOTH       -        R   Smoothed data value - returned in IRAWDT
C
C EXTERNAL REFERENCES: None
C
C STANDARDS VIOLATIONS: None.
C
C ENVIRONMENT:  DEC RSX-11M, FORTRAN 77
C
C DEVELOPMENT HISTORY:
C       DATE   INITIALS   DESCRIPTION
```

```
C     11/16/83   TML     Initial design
C     12/01/83   RVW     Added 3-pt. algorithm
C     01/11/84   TML     Loop through 3-pt. algorithm MODE times
C
C AUTHORS:  Ted Lichtenstein, Informatics General Corp.
C           Russell V. Westphal, NASA-Ames Research Center
C
C-************************************************************************

      INTEGER   IRAWDT(NRAWMX)

      IF(MODE.GT.0) GO TO 250

C**** MODE=0 : exponential smoothing (single-pole causal filter) ****

C  *  If the smoothing factor is 0. or out of range, just return:

      IF ( FACTOR.LE.0. ) GO TO 999
      IF ( FACTOR.GT.1. ) GO TO 999

C  *  Do the smoothing:

      FACT1M = 1. - FACTOR
      SMOOTH = FLOAT( IRAWDT(1) )

      DO 200 I = 1, NRAWMX
         SMOOTH = SMOOTH*FACTOR + FLOAT( IRAWDT(I) )*FACT1M
         IRAWDT(I) = INT( SMOOTH+.5 )
 200  CONTINUE
      GO TO 999

C**** MODE=1 : 3-pt. smoothing algorithm ****

 250  CONTINUE
      IMAX=NRAWMX-1

C  *  Loop through the 3-pt. algorithm, MODE no. of times:

      DO 400 J=1,MODE
         OLD=FLOAT(IRAWDT(1))
         DO 300 I=1,IMAX
            SMOOTH=(OLD+FLOAT(2*IRAWDT(I)+IRAWDT(I+1)))/4.0
            OLD=FLOAT(IRAWDT(I))
            IRAWDT(I)=INT(SMOOTH+0.5)
 300     CONTINUE
         SMOOTH=(OLD+3.0*FLOAT(NRAWMX))/4.0
         IRAWDT(NRAWMX)=INT(SMOOTH+0.5)
 400  CONTINUE

 999  RETURN
      END
```

```
C+----------------------------------------------------------------------
C
      SUBROUTINE SCZERO ( IRAWDT, NRAWMX, MINFIT, MAXFIT, NINTMN,
     >                    AVG, RMS, RMSFCT, ZERO, NZEMAX, NZERO )
C
C ACRONYM:  Standard Computations - find ZEROes
C           -        -                ----
C
C PURPOSE:
C           Find mean, standard deviation of data array in the interval
C           defined by MINFIT, MAXFIT. Then locate positively-sloped
C           zeroes of the data array in the interval.
C
C METHOD:
C           Average and standard deviation are found using simple
C           running sums of the smoothed data array.
C           Zeroes are found by bracketing regions where all the data
C           lie within a specified fraction of the standard deviation
C           of the mean and the slope of the curve is positive.
C           Then a straight line is fit to the region so located and
C           the zero-crossing is computed from this fit.
C
C ARGUMENTS
C    ARG        DIM      TYPE I/O/S DESCRIPTION
C   IRAWDT     NRAWMX     I     I   The raw data
C   NRAWMX       -        I     I   Length of raw data array.
C   MINFIT       -        I    I/O  Minimum argument for data reduction.
C                                    Normally an input variable, but it will be
C                                    reset if out of range.
C   MAXFIT       -        I    I/O  Maximum                 "
C   NINTMN       -        I     I   Min. no. of points in one interval used to
C                                    determine the zero-crossing line (>= 1).
C   AVG          -        R     O   Average of smoothed signal counts.
C   RMS          -        R     O   Standard deviation of smoothed signal counts.
C   RMSFCT       -        R     I   Fraction of RMS to use for testing if a given
C                                    data point is in the region near a zero.
C   ZERO       NZEMAX     R     O   Abscissa locations where smoothed input wave
C                                    IRAWDT has a positive-sloped zero.
C   NZEMAX       -        I     I   Amount of storage for ZERO(*) in the calling
C                                    program, in 4-byte array elements.
C   NZERO        -        I     O   No. of zeroes found.
C
C COMMONS USED: None
C
C FILES USED: None
C
C ERROR HANDLING:
C       Stop if there is not enough storage for the zero-crossings.
C
C NOTES:
C (1)   The zero-finder requires reasonably smooth data and a constant
C       mean-line to work properly.
C (2)   The routine may find one zero outside the interval on each side
C       if there are data near the zero just within the interval. These
C       should be valid zeroes, although the calling program may elect
C       to discard them.
C
C EXTERNAL REFERENCES:  None
C
C STANDARDS VIOLATIONS: None.
```

```
C
C ENVIRONMENT:  DEC RSX-11M, FORTRAN 77
C
C DEVELOPMENT HISTORY:
C       DATE    INITIALS    DESCRIPTION
C     11/16/83    RVW       Initial design and coding
C     01/12/84    TML       Modified
C     10/19/84    RVW       Improved checking of intervals
C
C AUTHOR:  Russell V. Westphal, NASA-Ames Research Center
C          Ted Lichtenstein, Informatics General Corp.
C
C-----------------------------------------------------------------------

      REAL      AVG, RMS, ZERO(NZEMAX)
      INTEGER   IRAWDT(NRAWMX)

C  *  Make sure that MINFIT and MAXFIT are in range, by resetting any
C  *  out of range value:

      IF ( MINFIT.LT.1 ) MINFIT = 1
      IF ( MAXFIT.GT.NRAWMX ) MAXFIT = NRAWMX

C  *  Test RMSFCT and NINTMN to be sure they're reasonable

      IF ((RMSFCT.LT.0.1).OR.(RMSFCT.GT.2.)) GO TO 990
      IF ((NINTMN.LT.1).OR.(NINTMN.GT.10)) GO TO 990

C  *  Average the smoothed data to find the mean line on the interval;
C     also, compute the rms of the (possibly smoothed) signal

      AVG=0.0
      RMS = 0.0
      DO 300 I=MINFIT,MAXFIT
         IIND = I - MINFIT + 1
         AVG = AVG + (FLOAT(IRAWDT(I))-AVG)/FLOAT(IIND)
         DEVIAT = FLOAT( IRAWDT(I) ) - AVG
         RMS = RMS + (DEVIAT*DEVIAT-RMS)/FLOAT(IIND)
 300  CONTINUE
      RMS = SQRT( RMS )

C  *  Search the data for regions which contain positive-sloped zeroes;
C     bracket these regions and locate the zeroes

      NZERO=0
      IENFL=0
      NIN  =0

C *** START OF SEARCH LOOP ***

      DO 500 I=MINFIT,MAXFIT

C    -- See if point is in the region near a zero

         IF(ABS(FLOAT(IRAWDT(I))-AVG).LT.(RMS*RMSFCT)) GO TO 410

C    -- Now if the region has been bracketed, go to fitting algorithm

 402     CONTINUE
         IF((IENFL.EQ.1).AND.(NIN.GE.NINTMN)) GO TO 420
```

```
C    -- Continue search for more zeroes

 405      CONTINUE
          IENFL=0
          NIN=0
          GO TO 490

C    -- Loop to bracket a contiguous region near zero

 410      CONTINUE
          IF(IENFL.EQ.0) IMIN=I    !first point in interval is IMIN
          IMAX=I
          NIN=IMAX-IMIN+1
          IENFL=1

C    -- If this is the last point in the interval, check if
C       there's a zero in the bracketed region:

          IF ( I.EQ.MAXFIT ) GO TO 402
          GO TO 490

C    -- Fit data near zero to straight line and find zero crossing

 420      CONTINUE

C    -- Check that first point in this region is below the mean line,
C    -- and last point is above the mean line:

          IF ( FLOAT( IRAWDT(IMIN) ).GE.AVG ) GO TO 405
          IF ( FLOAT( IRAWDT(IMAX) ).LE.AVG ) GO TO 405

          SX=0.0
          SY=0.0
          SXX=0.0
          SXY=0.0
          DO 450 JJ=IMIN,IMAX
             RJJ = FLOAT(JJ-IMIN)
             SX=SX+RJJ
             SXX=SXX+RJJ*RJJ
             SY=SY+FLOAT(IRAWDT(JJ))-AVG
             SXY=SXY+(FLOAT(IRAWDT(JJ))-AVG)*RJJ
 450      CONTINUE
          D=FLOAT(NIN)*SXX-SX*SX
          A=(SXX*SY-SX*SXY)/D
          B=(FLOAT(NIN)*SXY-SX*SY)/D
          ZDUM=-A/B+FLOAT(IMIN)

C    -- Check to be sure the zero is positively sloped, and is
C       in the interval [IMIN, IMAX]

          WRITE(4,3000) B,IMIN,IMAX,ZDUM
3000      FORMAT(' B = ',E15.7,' IMIN = ',I5,' IMAX = ',I5,
     >           ' ZERO : ',E15.7)

          IF(B.LE.0.) GO TO 405
          IF((ZDUM.LT.FLOAT(IMIN)).OR.(ZDUM.GT.FLOAT(IMAX)))
     >    GO TO 405

C    -- If so, add it to the list of positive-sloped zeroes found
```

```
          NZERO=NZERO-1

C    -- Stop if we have run out of storage space:

          IF ( NZERO.GT.NZEMAX ) STOP 'SCZERO: LACK OF STORAGE'

          ZERO(NZERO)=-A/B+FLOAT(IMIN)
          GO TO 405

 490      CONTINUE
 500  CONTINUE

C *** END OF SEARCH LOOP ***
      GO TO 999

 990  STOP 'SCZERO : BAD ARGUMENT VALUE'

 999  RETURN
      END
```

```
C-----------------------------------------------------------------------
C
      SUBROUTINE SCCFIT ( ZEROP, NZEROP, MODE, CFNFP, ASLFP,
                          TSTFP , ERROR )
C
C ACRONYM:  Standard Computations - Curve FIT zero locations
C           -        -               -     ---
C
C PURPOSE:
C           Fit locations of a particular phase of a periodic waveform
C           to the LOFI data reduciton equation.
C
C METHOD:
C           Fit of the LOFI data reduction equation:
C
C           ASLFP =average of (CFNFP-I)*(TSTFP+ZEROP(I)) for I=1,NZEROP
C
C           The problem is to minimize the rms error of the computed
C           fringe-time product with variable initial fringe number
C           and base time. A grid least-square routine (GRIDLS) is
C           used to perform the minimization.
C
C ARGUMENTS:
C    ARG        DIM      TYPE I/O/S DESCRIPTION
C   ZEROP       200       R     I   Abscissa locations where smoothed input wave
C                                     IRAWDT has a positive-sloped zero, ordered
C                                     in time (high to low fringe numbers)
C   NZEROP       -        I     I   No. of zeroes in data array
C   MODE         -        I     I   Used to specify whether initial time base
C                                     is to be fit or input:
C                                     MODE=1 : TSTFP is input
C                                     MODE=2 : TSTFP found from fit procedure
C   CFNFP        -        R     O   Fringe number offset
C   ASLFP        -        R     O   Product of time and fringe number (ANSWER)
C   TSTFP        -        R     O   Time base (from fit or input)
C   ERROR        -        R     O   RMS error of fit
C
C COMMONS USED:
C   /FITCOM/      Used locally to pass parameters to optimization routine
C
C FILES USED:   None
C
C ERROR HANDLING: None
C
C NOTES:
C  (1) A simple grid-search minimization routine is used for the
C      2-parameter minimization problem.
C
C LOCAL VARIABLES:
C    VAR        DIM      TYPE DESCRIPTION
C   ABSERR       -        R    Absolute error convergence criteria.
C   TOL          -        R    Convergence criteria on error variation
C                              between successive calls to GRIDLS
C   ITMAX        -        I    Maximum no. of calls to GRIDLS allowed
C   ERRMAX       -        R    Allowable error if ITMAX is equalled
C
C EXTERNAL REFERENCES:
C    NAME        DESCRIPTION AND SOURCE
C   FITERR       Function called by GRIDLS to evaluate error of fit
C   GRIDLS       Grid-search function minimization routine
```

```
C
C STANDARDS VIOLATIONS: None.
C
C ENVIRONMENT:  DEC PDP-11/RSX-11M and VAX/VMS, FORTRAN 77.
C
C DEVELOPMENT HISTORY:
C       DATE    INITIALS    DESCRIPTION
C     11/30/83    RVW       Initial design
C     3/20/84     RVW       Implemented improved algorithm and numerics
C     10/19/84    RVW       Augmented convergence criteria
C
C AUTHOR:  Russell V. Westphal, NASA-Ames Research Center
C
C---------------------------------------------------------------------

      REAL       ZEROP(200)
      REAL       PARAM(2),DELTA(2)
      DATA       ABSERR/0.0025/, TOL/0.00005/, ERRMAX/0.05/
      DATA       ITMAX/100/
      COMMON/FITCOM/ CFNFIT,ASLFIT,TSTFIT,ZERO(200),NZERO,RMSERR
      EXTERNAL   FITERR

      NZERO=NZEROP
      DO 5 I=1,NZERO
 5    ZERO(I)=ZEROP(I)

C * Initial guesses for grid optimizer along with step sizes for search
C * NOTE: its easy to guess the initial fringe number, but quite difficult
C        to estimate the basis time (MODE=2). The values selected will
C        only work well if the basis time is near zero, i.e., if the
C        fringe record begins approximately at the start of the oil flow.

      CFNFIT=FLOAT(NZERO)            ! lower bound on initial fringe number
      IF(MODE.EQ.1) TSTFIT=TSTFP     ! time base is input (MODE=1)
      IF(MODE.EQ.2) TSTFIT=0.0       ! guess for time base (MODE=2)
      DELTA(1)=1.0                   ! initial search grid size is one fringe
      DELTA(2)=ZERO(2)-ZERO(1)       ! set time grid size to least samples
                                     ! between zeroes

      PARAM(1)=CFNFIT
      PARAM(2)=TSTFIT
      OLDERR=FITERR(MODE,PARAM)
      ITNO = 0

 15   ITNO = ITNO + 1
      CALL GRIDLS(MODE,PARAM,DELTA,DUM,FITERR)
      WRITE(5,2000) ITNO, DUM
 2000 FORMAT( ' Iteration no.= ', I5, ' Error = ', F12.5 )
      CFNFIT=PARAM(1)
      TSTFIT=PARAM(2)

C * Convergence criteria:
C   ++ Error is less than a value ABSERR (acceptable error criteria);
C      OR
C   ++ Successive values of the error are the same within a small
C      fraction TOL of each other;
C      OR
C   ++ The routine has not converged after a large number of calls
C      to the grid-search routine, but the error is not terribly large.
C * IF ‹no convergence as defined› THEN STOP
```

```
C    NOTE: GRIDLS automatically adjusts grid search size for
C          successive calls.

      IF(DUM.LT.ABSERR) GO TO 20
      IF(ABS(DUM-OLDERR).LT.TOL) GO TO 20
      IF((ITNO.GT.ITMAX).AND.(DUM.LT.ERRMAX)) GO TO 20
      IF(ITNO.GT.ITMAX) GO TO 990
      OLDERR=DUM
      GO TO 15

C * Set values for return to calling program

20    CFNFP=CFNFIT
      ASLFP=ASLFIT
      TSTFP=TSTFIT
      ERROR=DUM
      GO TO 999

C * Error return

 990  CONTINUE
      STOP 'SCCFIT: NO CONVERGENCE'
 999  RETURN
      END

      REAL FUNCTION FITERR(MODE,PARAM)
      REAL PARAM(2)
      COMMON/FITCOM/ CFNFIT,ASLFIT,TSTFIT,ZERO(200),NZERO,RMSERR

C * Used to compute relative rms error of the fringe-time product
C   from the average value of this quantity using input values
C   of initial fringe number PARAM(1) and time base PARAM(2).

      CFNFIT=PARAM(1)
      IF(MODE.EQ.2) TSTFIT=PARAM(2)

C * Compute rms error of the fit

      SC=0.
      SCC=0.

        DO 1 I=1,NZERO

C --- Fringe-time product for ith zero

        CI=(CFNFIT-FLOAT(I))*(ZERO(I)+TSTFIT)

C --- Running-sum averages for mean and std. deviation

        SC  = SC  + ( CI  - SC  ) / FLOAT(I)
        SCC = SCC + (CI*CI- SCC ) / FLOAT(I)
 1      CONTINUE

C * RMS error of fit is std. deviation of fringe-time product
C   coputed for each zero crossing

      RMSERR=SQRT(SCC-SC*SC)

C * Average fringe-time product is taken as the answer
```

```
      ASLFIT=SC

C * The RELATIVE error is the quantity which is being minimized

      FITERR=RMSERR/ASLFIT

      RETURN
      END

C+----------------------------------------------------------------
C SUBROUTINE GRIDLS
C
C PURPOSE    : Grid search for multi-dimensional minimization
C              problems such as least-square fitting.
C
C SOURCE     : P. R. Bevington, "Data Reduction and Analysis for
C              the Physical Sciences", McGraw-Hill, pp. 212-213;
C              modified by R. V. Westphal, 12/83
C
C USAGE      :
C               CALL GRIDLS ( NTERMS, A, DELTAA, CHISQR, FCHISQ )
C
C      NTERMS       No. of parameters
C      A            Parameter array
C      DELTAA       Increments for parameters
C      CHISQR       Error of fit
C      FCHISQ       Function to minimize
C
C FUNCTIONS CALLED:
C      FUNCTION FCHISQ ( NTERMS, A )   -- evaluates fit error
C
C NOTES      :
C      The calling program deals with convergence of the search,
C      typically by repeatedly calling GRIDLS and testing whether
C      CHISQR has attained a constant value (within some tolerance)
C      for two successive iterations. Note that the ever-smaller
C      values for the grid steps are automatically provided by the
C      subroutine on return to the caller (see statement 84).
C
C----------------------------------------------------------------

       SUBROUTINE GRIDLS(NTERMS,A,DELTAA,CHISQR,FCHISQ)
       DIMENSION A(NTERMS),DELTAA(NTERMS)
       CHISQR=0.
         DO 90 J=1,NTERMS
         CHISQ1=FCHISQ(NTERMS,A)
         FN=0.
         DELTA=DELTAA(J)
41       A(J)=A(J)+DELTA
         CHISQ2=FCHISQ(NTERMS,A)
         IF(CHISQ1-CHISQ2) 51,41,61
51       DELTA=-DELTA
         A(J)=A(J)+DELTA
         SAVE=CHISQ1
         CHISQ1=CHISQ2
         CHISQ2=SAVE
61       FN=FN+1.
         A(J)=A(J)+DELTA
         CHISQ3=FCHISQ(NTERMS,A)
```

```
          IF(CHISQ3-CHISQ2) 71.81.81
71        CHISQ1=CHISQ2
          CHISQ2=CHISQ3
          GO TO 61
81        DELTA=DELTA*(1./(1.+(CHISQ1-CHISQ2)/(CHISQ3-CHISQ2))+0.5)
          A(J)=A(J)-DELTA
84        DELTAA(J)=DELTAA(J)*FN/3.
90        CONTINUE

C * Minimum has been located - evaluate function and return

        CHISQR=FCHISQ(NTERMS,A)

        RETURN
        END
```

```
C+----------------------------------------------------------------
C
      SUBROUTINE SCLOFI ( TCOIL, TCNOM, MUNOM, NOIL, WLLSER,
     >                    ANGIN, DXBEAM, DELNT, TAUBAR, IER )
C
C ACRONYM:  Standard Computations - Laser Oil Film Interferometer
C           -        -                -     -   -    -
C
C PURPOSE:
C           Implement lubrication theory data reduction equation for
C           laser oil film interferometry measurement of skin friction.
C           For use with Dow-Corning 200 silicone oil and applicable
C           to both single- and two-beam interferometers.
C
C METHOD:
C           Simply compute the skin friction from the linear equation.
C           Oil viscosity is computed from the Dow-Corning exponential
C           relation, and the effective incidence angle is computed
C           from the equation for geometric optics.
C
C ARGUMENTS:
C    ARG        DIM     TYPE I/O/S DESCRIPTION
C   TCOIL        -        R    I   Oil temperature, in C.
C   TCNOM        -        R    I   Nominal oil temperature for D-C
C                                    equation, in C.
C   MUNOM        -        R    I   Nominal oil viscosity for D-C
C                                    equation, in Kg/(m-s).
C   NOIL         -        R    I   Oil index of refraction
C                                    NOIL = 1.4 nominally for D-C oil.
C   WLLSER       -        R    I   Laser wavelength in m.
C                                    WLLSER = 0.6328 X 10^-6 for He-Ne.
C   ANGIN        -        R    I   Laser incidence angle, in deg.
C                                    ANGIN = 0. for normal incidence.
C   DXBEAM       -        R    I   Beam separation in m. For single-beam
C                                    LOFI, this is the distance from the
C                                    oil film leading edge.
C   DELNT        -        R    I   1/(difference in fringe-time product)
C                                    in units of 1/(fringe-s).
C   TAUBAR       -        R    O   The shear stress, in N/m^2
C   IER          -        I    O   Error return code.
C
C COMMONS USED: None
C
C FILES USED: None
C
C ERROR HANDLING:
C       Check range of inputs. IER=1 means no obvious input error.
C
C NOTES:
C (1)   This routine will only work for Dow-Corning oils!
C
C LOCAL VARIABLES:
C    VAR        DIM     TYPE DESCRIPTION
C   MUOIL        -        R   Oil viscosity from D-C equation, in N-s/m^2.
C   ANGOIL       -        R   Effective beam angle through oil, in rad.
C   OPLOIL       -        R   Optical path length in the oil, in m/fringe.
C
C EXTERNAL REFERENCES: None
C
C STANDARDS VIOLATIONS: None.
```

```
C
C ENVIRONMENT:  DEC VMS, FORTRAN 77
C
C DEVELOPMENT HISTORY:
C       DATE    INITIALS    DESCRIPTION
C      1/16/85    RVW      Initial design and coding
C
C AUTHOR:  Russell V. Westphal, NASA-Ames Research Center
C
C-----------------------------------------------------------------------

      REAL       PI
      PARAMETER (PI=3.1415926)
      INTEGER    IER
      REAL       TCOIL, TCNOM, MUNOM, NOIL, ANGIN, DXBEAM,
     >           DELNT, TAUBAR
      REAL       MUOIL, ANGOIL, OPLOIL

C  *  Initialize

      IER = 1

C  *  Range check inputs:

      IF((TCOIL.LT.0.).OR.(TCOIL.GT.100.)) GO TO 990
      IF((TCNOM.LT.-200.).OR.(TCNOM.GT.200.)) GO TO 990
      IF((MUNOM.LT.0.).OR.(MUNOM.GT.1.E6)) GO TO 990
      IF((WLLSER.LT.0.).OR.(WLLSER.GT.10.E-6)) GO TO 990
      IF((NOIL.LT.0.).OR.(NOIL.GT.5.)) GO TO 990
      IF((ANGIN.LT.0.).OR.(ANGIN.GT.90.)) GO TO 990
      IF((DXBEAM.LT.0.).OR.(DXBEAM.GT.1.)) GO TO 990
      IF((DELNT.LT.-1.E-6).OR.(DELNT.GT.1.E6)) GO TO 990

C  *  Viscosity from Dow-Corning formula -- kg/(m-s) = N-s/m^2

      MUOIL = MUNOM / (EXP(0.0146 * (TCOIL - TCNOM)))

C  *  Incidence angle -- rad

      ANGOIL = ASIN(SIN(PI*ANGIN/180.)/NOIL)

C  *  Optical path length in the oil -- m per fringe

      OPLOIL = WLLSER / (2. * NOIL * COS(ANGOIL))

C  *  Linear lubrication theory - equation for shear stress -- N/m^2

      TAUBAR = MUOIL * DXBEAM * DELNT / OPLOIL

      GO TO 999

 990  IER = 0

 999  RETURN

      END
```

REFERENCES

1. Squire, L. C.: In Flow Visualization in Wind Tunnels Using Indicators. AGARDograph vol. 70, Maltby, R. L., ed., Apr. 1962, pp. 7-55.

2. Tanner, L. H., and Blows, L. G.: A Study of the Motion of Oil Films on Surfaces in Air Flow, with Application to the Measurement of Skin Friction. J. Phys. E.: Sci. Inst., vol. 9, no. 3, Mar. 1976, pp. 194-202.

3. Murphy, J. D.; and Westphal, R. V.: The Laser-Interferometer Skin-Friction Meter: A Numerical and Experimental Study. Proc. 3rd Symposium on Numerical and Physical Aspects of Aerodynamic Flows, Jan. 9-11, 1985, Long Beach, CA.

4. Jenkins, F. A.; and White, H. E.: Fundamentals of Optics, Fourth ed., McGraw-Hill, 1976, pp. 286-299.

5. Murphy, J. S.; and Smith, A. M. O.: Measurement of Wall Shearing Stress in the Boundary Layer by Means of an Evaporating Liquid Film. J. Appl. Phys., vol. 27, no. 9, Sep. 1956, pp. 1097-1103.

6. Wazzan, A. R.; Smith, A. M. O.; and Lind, R. C.: Mass Transfer Method of Measuring Wall Shear Stress in Supersonic Flow. Phys. Fluids, vol. 8., no. 9, Sep. 1965, pp. 1641-1646.

7. Tanner, L. H.; and Kulkarni, V. G.: The Viscosity Balance Method of Skin Friction Measurement: Further Developments Including Applications to Three-Dimensional Flow. J. Phys. E.: Sci. Inst., vol. 9, no. 12, Dec. 1976, pp. 1114-1121.

8. Tanner, L. H.: A Skin Friction Meter, Using the Viscosity Balance Principle, Suitable for Use with Flat or Curved Metal Surfaces. J. Phys. E.: Sci. Inst., vol. 10, no. 3, Mar. 1977, pp. 278-284.

9. Tanner, L. H.: A Comparison of the Viscosity Balance and Preston Tube Methods of Skin Friction Measurement. J. Phys. E.: Sci. Inst., vol. 10, no. 6, June 1977, pp. 627-632.

10. Tanner, L. H.: A More Accurate Viscosity Balance Measurement of the Variation of Skin Friction with Reynolds Number, for Comparison with Preston Tubes. J. Phys. E.: Sci. Inst., vol. 10, no. 8, 1977, p. 843.

11. Tanner, L. H.: Skin Friction Measurements by Viscosity Balance in Air and Water Flows, J. Phys., E.: Sci. Inst., vol. 12, no. 7, July 1979, pp. 610-619.

12. Tanner, L. H.: The Application of Fizeau Interferometry of Oil Films to the Study of Surface Flow Phenomena. Optics and Lasers in Engrg., vol. 2, 1981, pp. 105-118.

13. Tanner, L. H.: Two Accurate Optical Methods for Newtonian Viscosity Measurements, and Observations on a Surface Effect with a Silicone Oil. J. Phys. E.: Sci. Inst., vol. 10, no. 10, 1977, pp. 1019-1028.

14. Monson, D. J.; and Higuchi, H.: Skin Friction Measurements by a New Nonintrusive Double Laser Beam-Oil Viscosity Balance Technique. AIAA J., vol. 19, no. 6, 1980, pp. 739-744.

15. Monson, D. J.; Driver, D. M.; and Szondruch, J.: Application of a Laser Interferometer Skin-Friction Meter in Complex Flows. ICIASF 1981 Record, 1981, pp. 232-243.

16. Monson, D. J.: A Non-Intrusive Laser Interferometer Method for Measurement of Skin Friction. Expts. in Fluids, vol. 1, no. 1, 1983, pp. 15-22.

17. Monson, D. J.: A Laser Interferometer for Measuring Skin Friction in Three-Dimensional Flows. AIAA J., vol. 22, no. 4, 1984, pp. 557-559.

18. Holman, J. P.: Experimental Methods for Engineers, Chapter 3, second edition, McGraw-Hill, 1971.

19. Hooper, C.; and Saunders, D.: FMDAS: Fluid Mechanics Data Acquisition System. Informatics General Corporation, Project No. 7014-307, Technical Note No. 13, 1985.

20. Tanner, L. H.: Camera Testing by Use of Speckle Patterns. Applied Optics, vol. 10, no. 9, pp. 2026-2034.

21. Coles, D.: The Young Person's Guide to the Data. Proceedings 1968 AFOSR-Stanford Conference on Computation of Turbulent Boundary Layers, vol. 2, D. Coles and E. Hirst, eds., pp. 1-19.

TABLE 1.- UNCERTAINTY ANALYSIS, TERM BY TERM BREAKDOWN

Data reduction equation: $\tau = \dfrac{\mu_o(X_2 - X_1)}{\lambda_o[C(X_2) - C(X_1)]}$

Linear, independent undertainty model: $\dfrac{\delta\tau}{\tau} = \sqrt{\sum_{i=1}^{4} \left(\dfrac{\delta T_i}{T_i}\right)^2}$

i	T_i	est $\delta T_i/T_i$	Conditions
1	μ_o	0.02	Flow temperature measured, manufacturer equation verified
2	λ_o	<0.005	Near-normal incidence measured n_o
3	$X_2 - X_1$	≤ 0.02*[a]	Beam spacing measured directly at focal plane
4	$C(X_2) - C(X_1)$	$\dfrac{\delta C}{C}\sqrt{\dfrac{1 + C_X^2}{(1 - C_X)^2}}$ [b,c]	C known to high accuracy

[a] Spacing can be measured to ±0.05 mm → 2% @ $X_2 - X_1 = 2.77$ mm, the smallest spacing used.

[b] $\delta C/C$ is the uncertainty in the determination of fringe-time product for a particular beam. $\delta C/C \sim 0.005$ under idealized conditions.

[c] $C_X = X_2/X_1 = C(X_2)/C(X_1)$ from equation (5). Note that

$$X_1 - X_o = \frac{C_X}{1 - C_X}(X_2 - X_1)$$

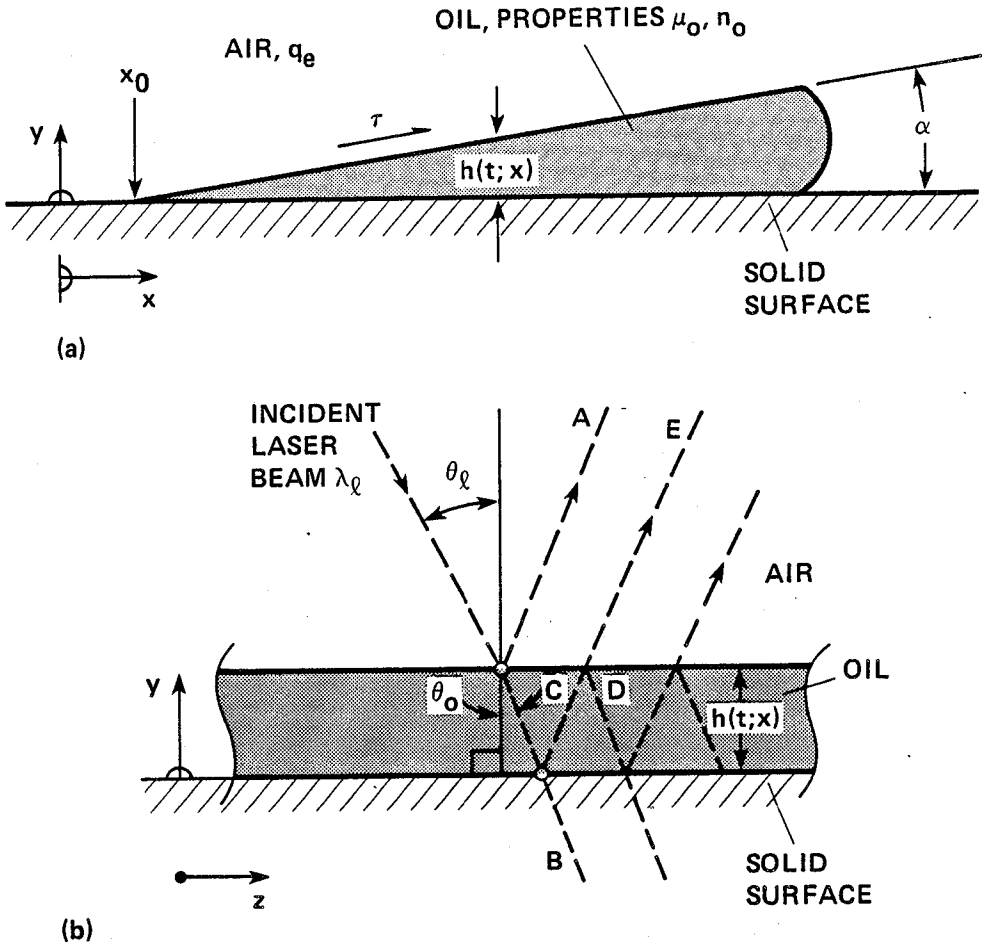

Figure 1.- Two dimensional oil film. (a) Coordinates and parameters for the film. (b) Laser interferometric measurement of oil film thickness.

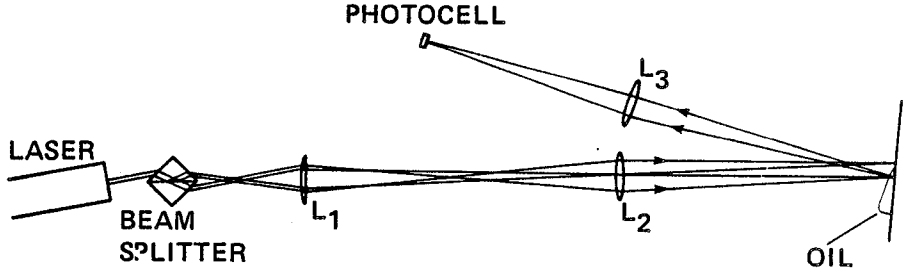

Figure 2.- Tanner's system (fig. 2 from ref. 12).

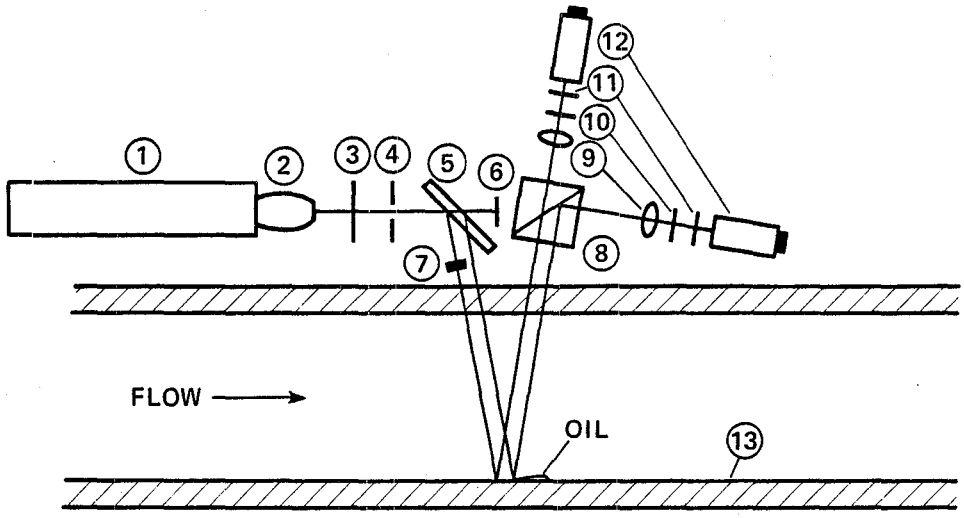

① He-Ne LASER
② TELESCOPE
③ NEUTRAL DENSITY FILTER
④ IRIS DIAPHRAGM
⑤ INTERFEROMETER FLAT
⑥ STOP
⑦ HALF-WAVE RETARDATION PLATE
⑧ POLARIZATION BEAM SPLITTER
⑨ FOCUSING LENS
⑩ POLARIZER
⑪ 6328 Å FILTER
⑫ SILICON PHOTODIODE
⑬ MODEL SURFACE

(a)

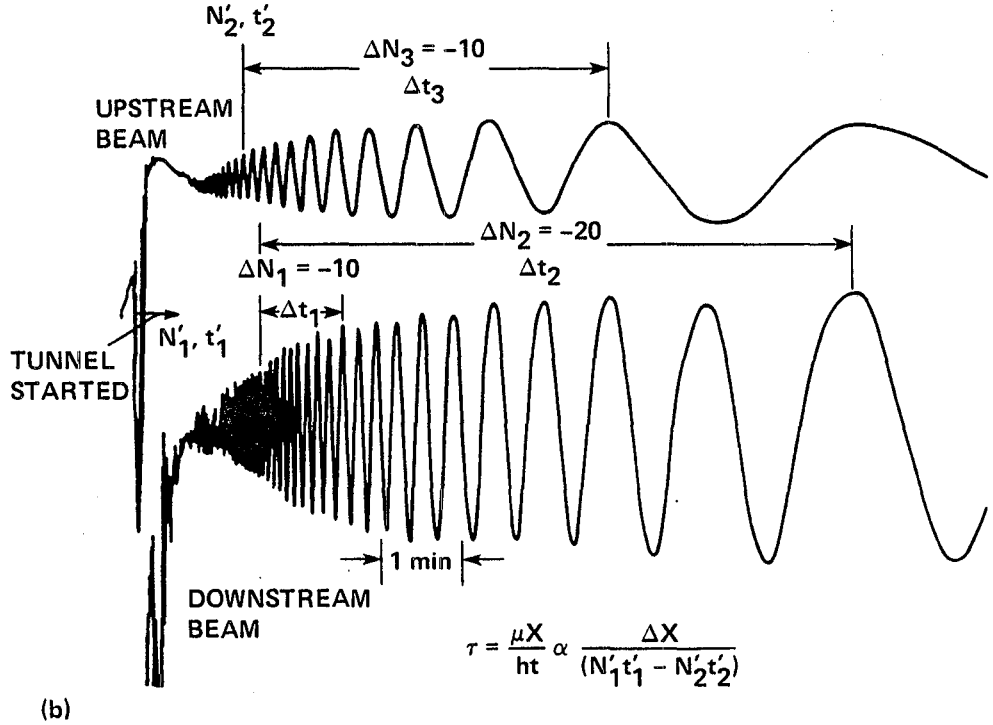

(b)

Figure 3.- Monson's oil film interferometer. (a) Monson's optical system (fig. 1 from ref. 14) showing major components. (b) Typical signal from Monson's instrument (fig. 2) from ref. 14), with data-reduction equations.

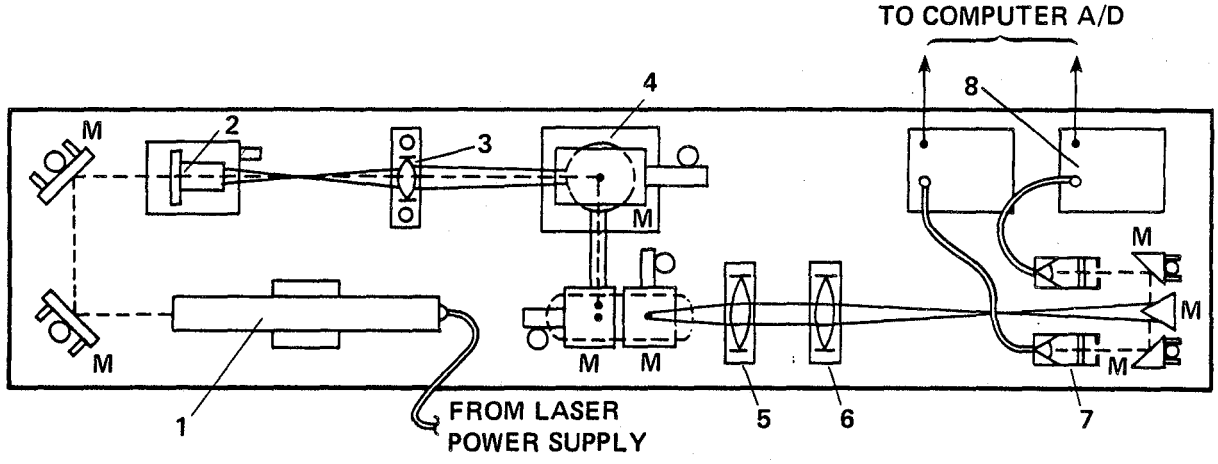

APPROX. SCALE
10 cm

PART NO.	DESCRIPTION	QTY
1	0.8 mW He-Ne LASER	1
2	20× OBJECTIVE	1
3	f150 mm ACHROMAT LENS	1
4	BEAMSPLITTER FIXTURE	1
5	COLLIMATING LENS f450	1
6	FOCUSING LENS f250	1
7	DETECTOR ASS'Y	2
8	PHOTODIODE AMPLIFIERS	2
M	MIRRORED SURFACES	8

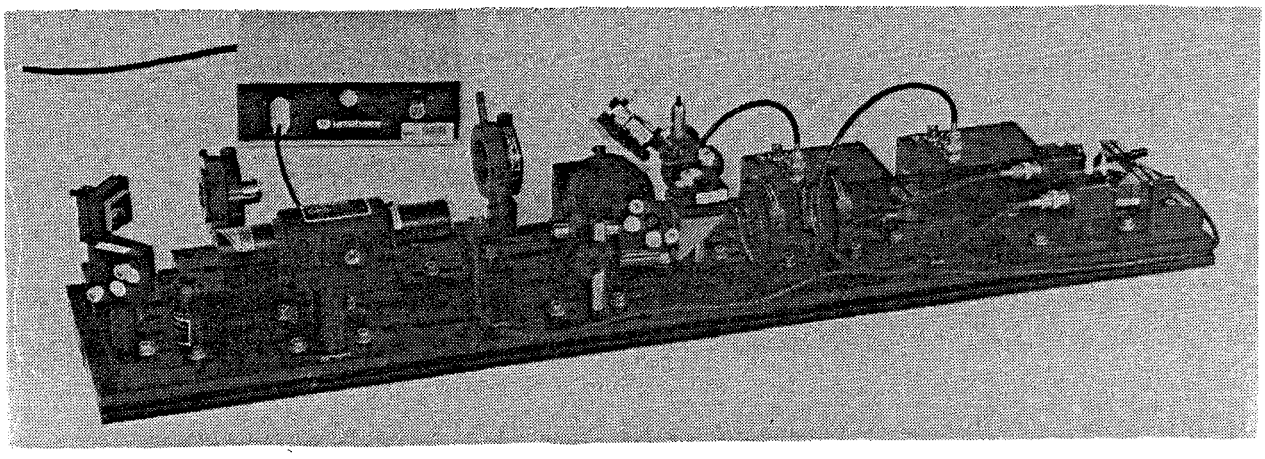

Figure 4.- Current optical hardware.

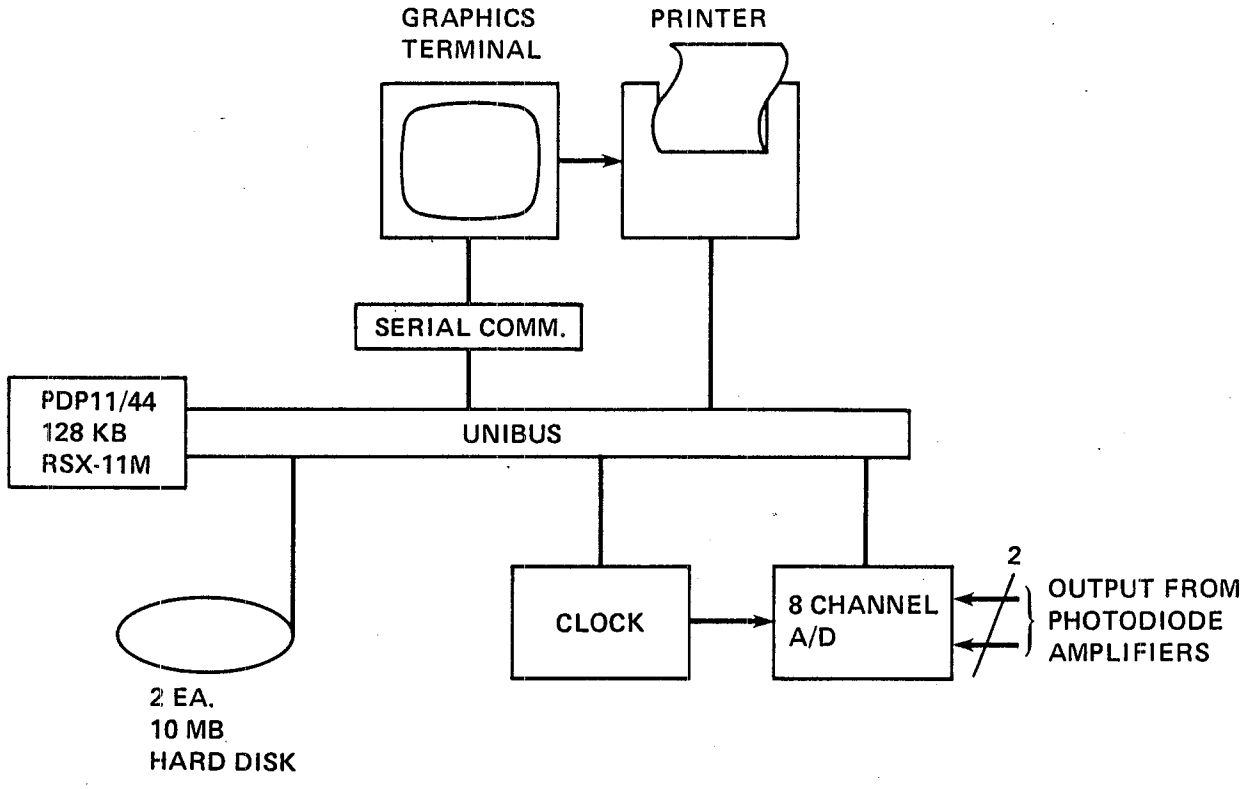

Figure 5.- Data-acquisition system.

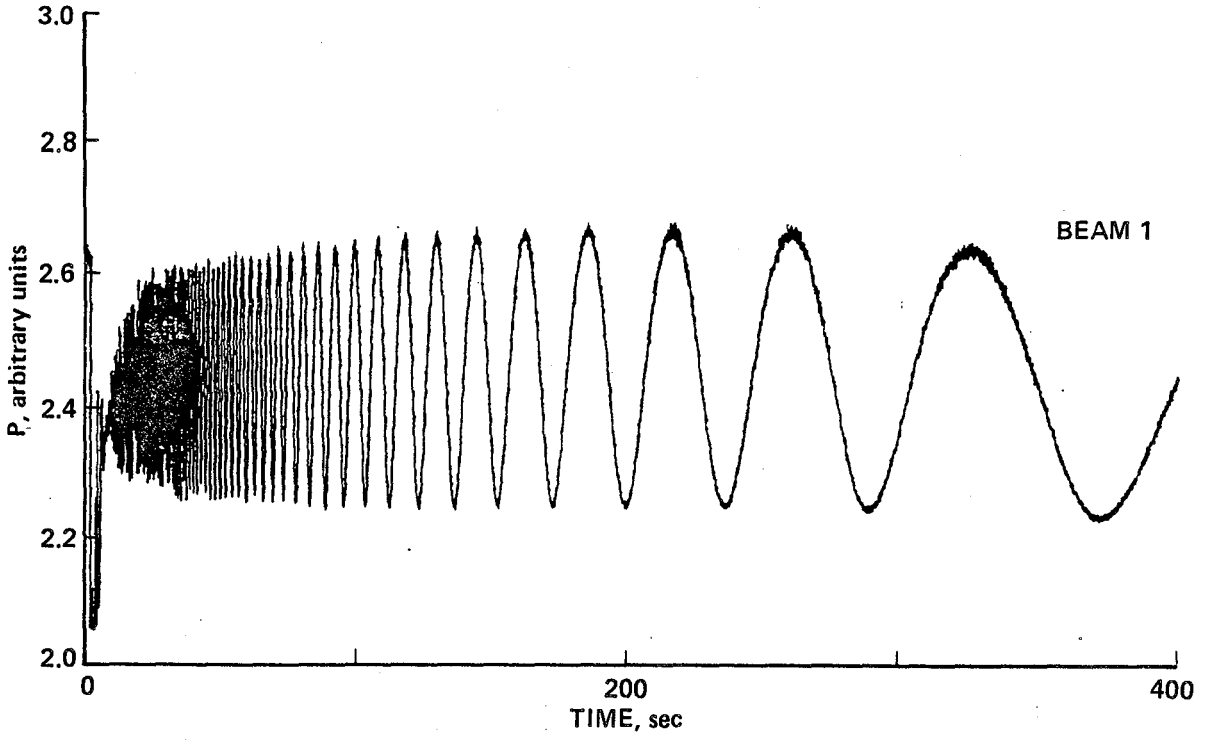

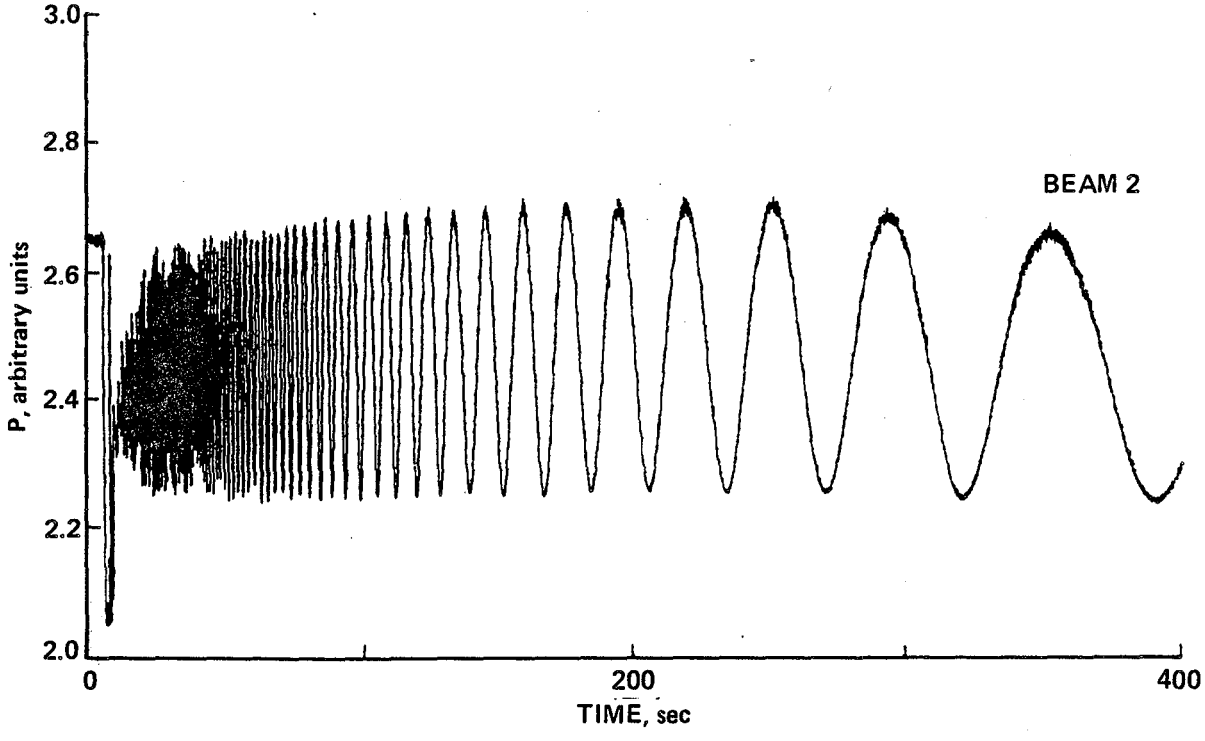

(a) Before processing. Note that the signal quality on each beam is equal, as provided by this design.

Figure 6.- Typical digitized photodetector signal.

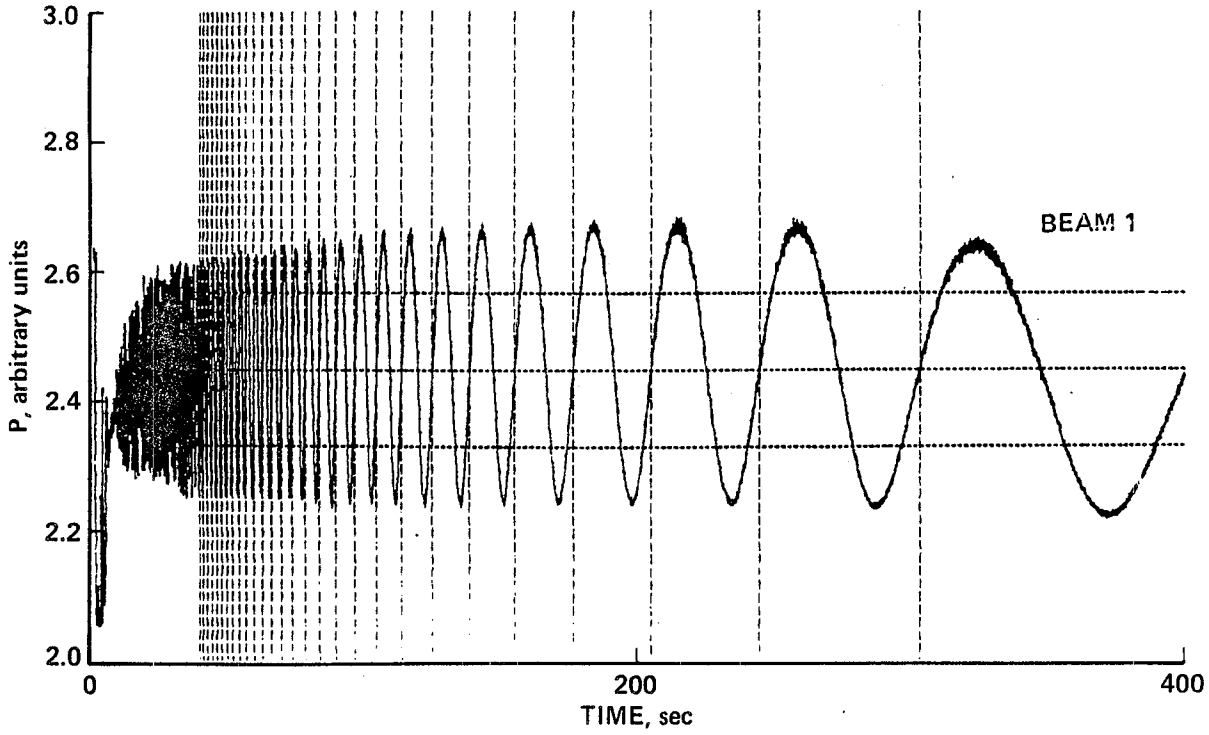

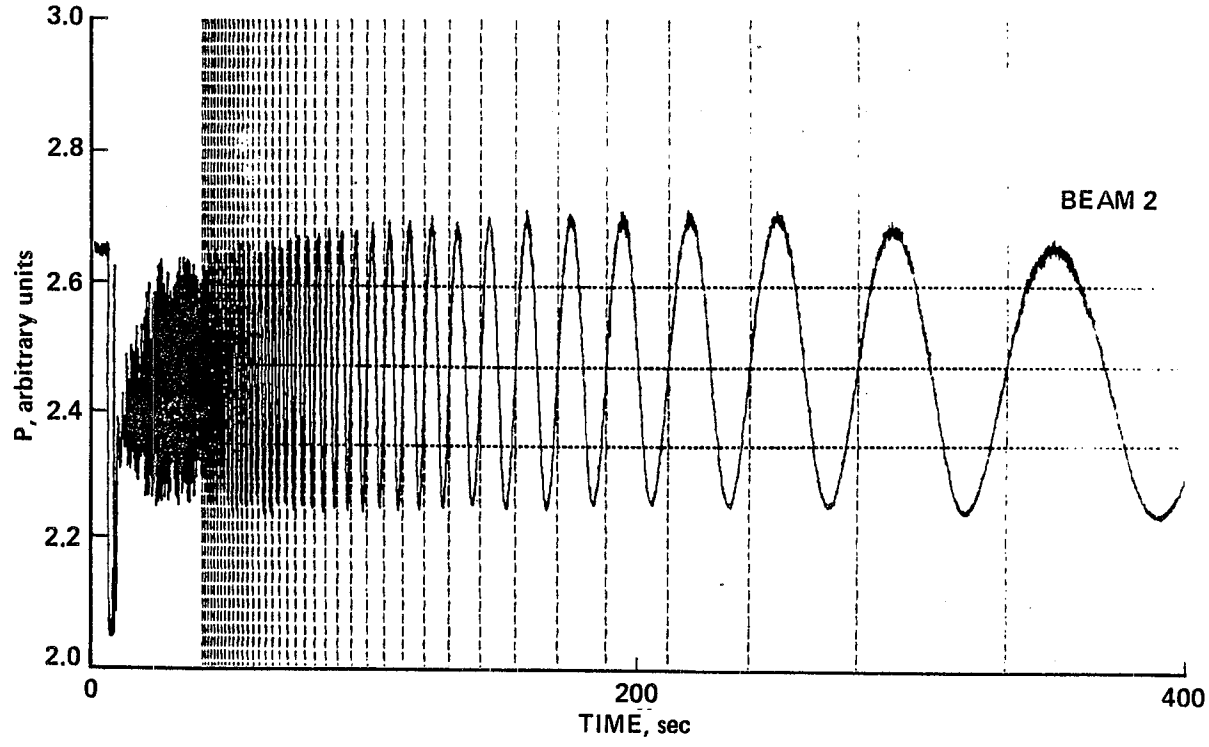

(b) Processed signal of figure 6a, showing fringe locations as identified by subroutine SCZERO.

Figure 6.- Continued.

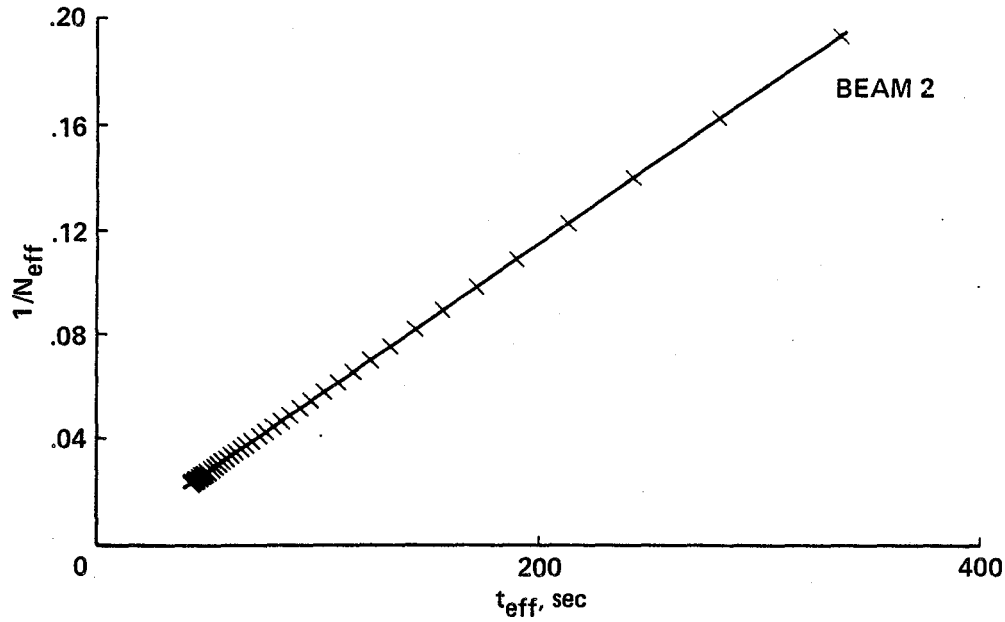

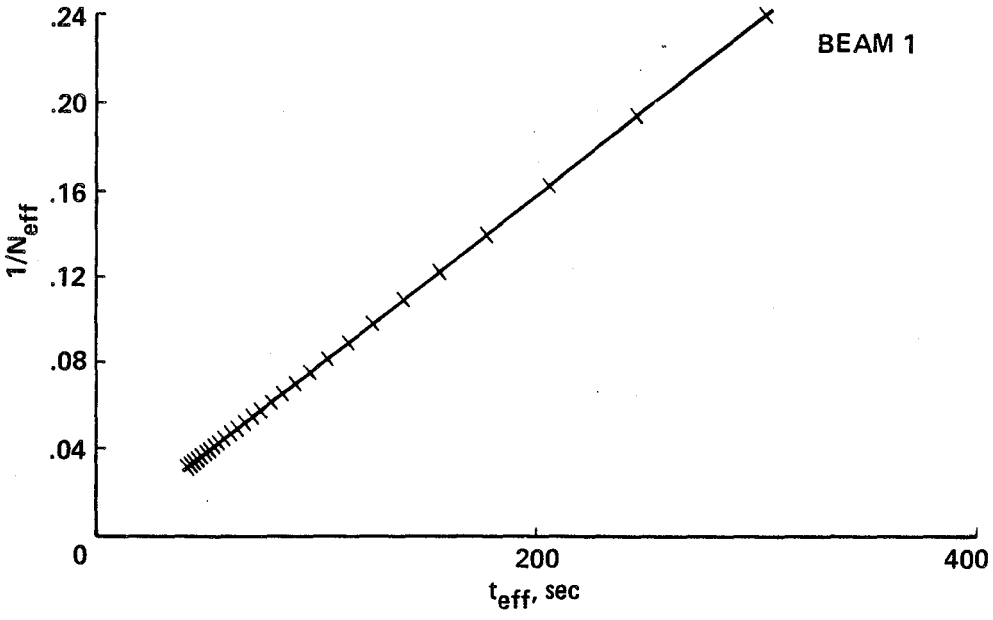

(c) Fit of fringe-time history to lubrication theory, from fringes identified in figure 6b, using subroutine SCCFIT.

Figure 6.- Concluded.

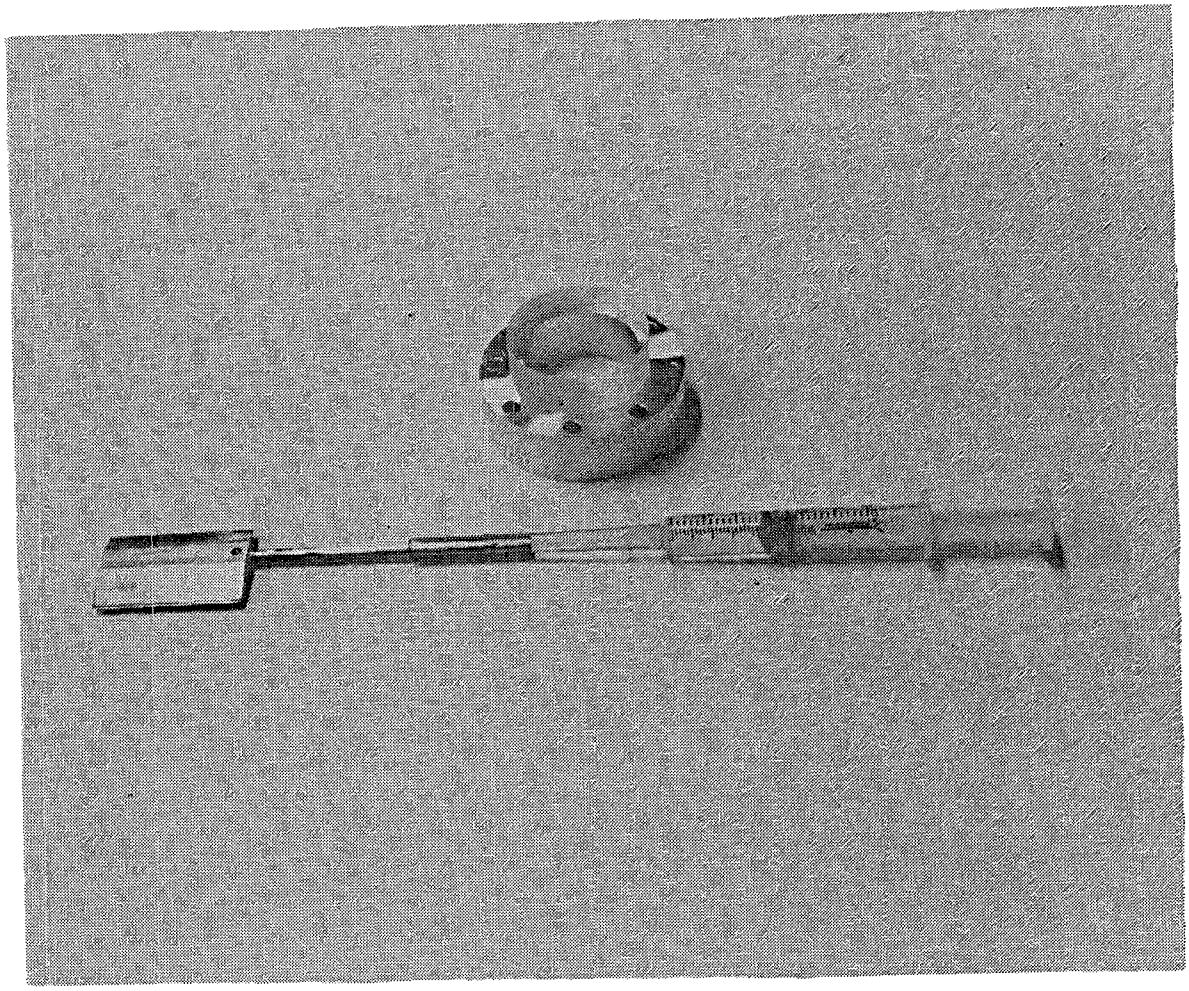

Figure 7.- Special oil applicator fixture and metal-coated glass-surface insert.

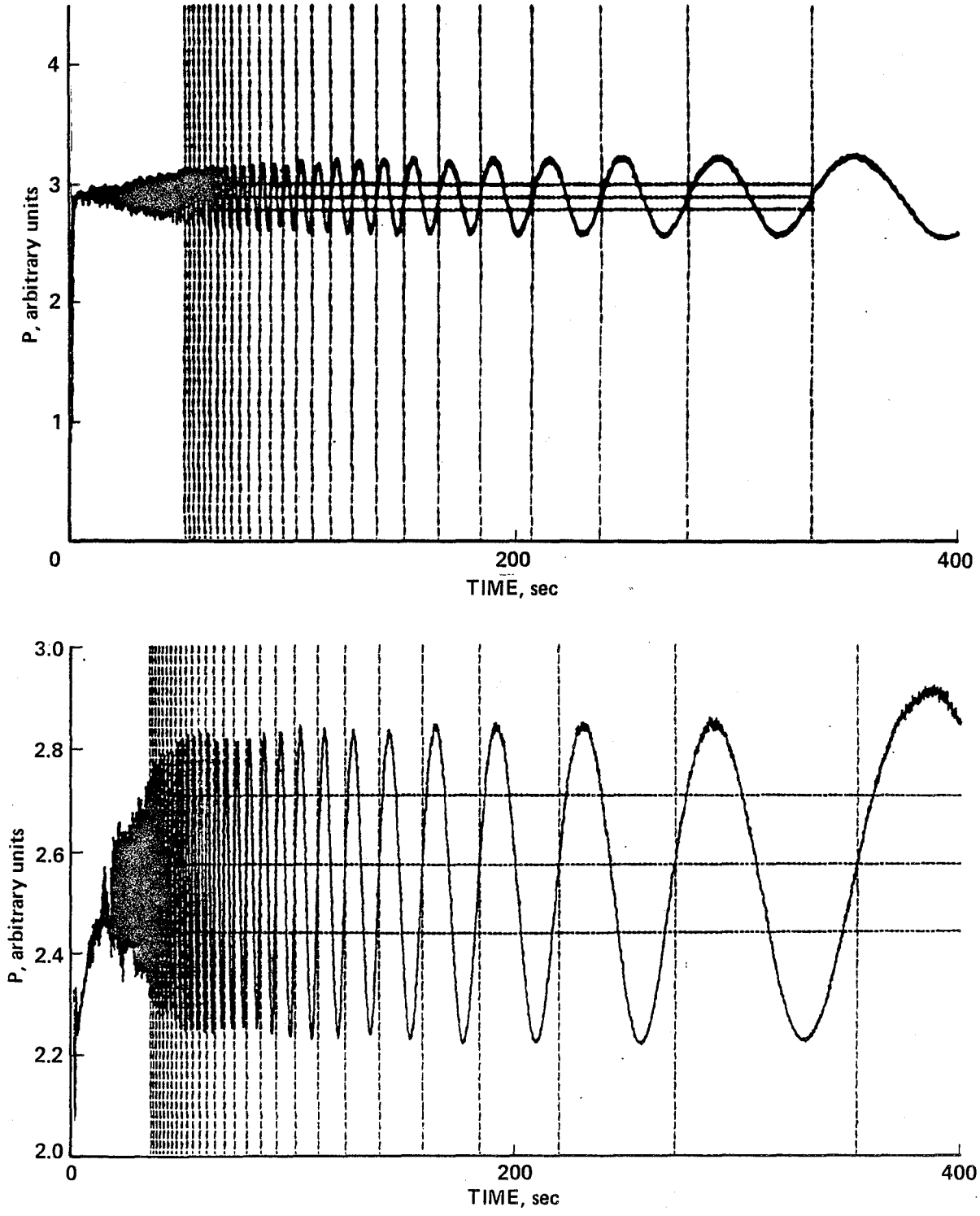

Figure 8.- Signal visibility. (a) Results on polished aluminum. (b) Compared to metal-coated glass surface.

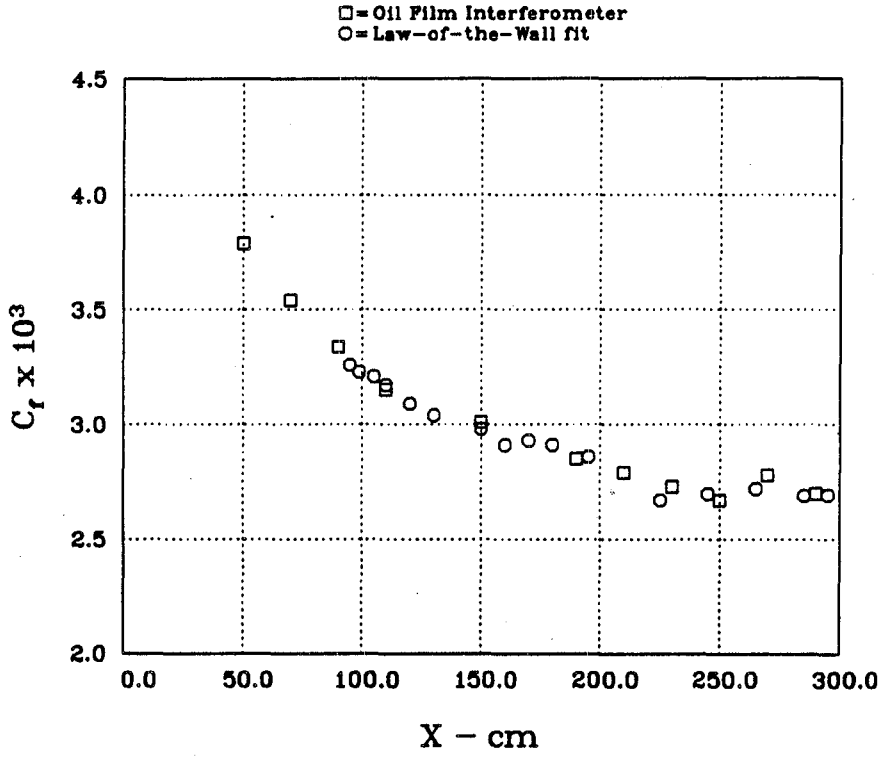

Figure 9.- Skin friction in constant-pressure turbulent boundary layer.

1. Report No.	2. Government Accession No.	3. Recipient's Catalog No.
NASA TM 88216		

4. Title and Subtitle	5. Report Date
IMPROVED SKIN FRICTION INTERFEROMETER	March 1986
	6. Performing Organization Code

7. Author(s)	8. Performing Organization Report No.
R. V. Westphal,[1] W. D. Bachalo,[2] and M. H. Houser[2]	A-86138
	10. Work Unit No.

9. Performing Organization Name and Address	11. Contract or Grant No.
[1]NASA Ames Research Center, Moffett Field, CA 94035 [2]Aerometrics Inc., Mountain View, CA	
	13. Type of Report and Period Covered
12. Sponsoring Agency Name and Address	Technical Memorandum
National Aeronautics and Space Administration Washington, DC 20546	14. Sponsoring Agency Code 505-60-31

15. Supplementary Notes

Point of Contact: R. V. Westphal, Ames Research Center, M/S 227-8, Moffett Field, CA 94035, (415)694-5856 or FTS 464-5856

16. Abstract

An improved system for measurement of aerodynamic skin friction using a dual laser beam oil film interferometer has been developed. Improvements to the optical hardware provided equal signal characteristics for each beam and reduced the cost and complexity of the system by replacing polarization rotation by a mirrored prism for separation of the two signals. An automated, objective data reduction procedure was implemented to eliminate tedious manual manipulation of the interferometry data records. Although the present system was intended for use in two-dimensional, incompressible flow over a smooth, level surface without pressure gradient, the improvements discussed are not limited to this application.

17. Key Words (Suggested by Author(s))	18. Distribution Statement
Skin friction Interferometry Oil film Boundary layer Interferometer	Unlimited Subject Category - 035

19. Security Classif. (of this report)	20. Security Classif. (of this page)	21. No. of Pages	22. Price*
Unclassified	Unclassified	45	A03

*For sale by the National Technical Information Service, Springfield, Virginia 22161

End of Document